OPALE: Operational assessment of landscape water eco-functionalities

D. Trévisan, P. Taillandier, Benoit Sarrazin, D. Etienne, N. Ayari, C. Petiqueux, P. Quétin, C. Janin

OPALE: OPerational Assessment of Landscape water Eco-functionalities

D. Trévisan [a,b,*], P. Taillandier [c,d,e], B. Sarrazin [f], D. Etienne [g], N. Ayari [c], C. Petiqueux [h], P. Quétin [a], C. Janin [i]

[a] INRAE UMR Carrtel, 75 avenue de Corzent, BP 511 F74203 Thonon les bains, France.

[b] INRAE UMR iEES, 4 place Jussieu F75252 Paris Cedex

[c] INRAE UR MIAT, Toulouse, France

[d] IRD/SU UMI UMMISCO, Hanoi, Vietnam

[e] Thuyloi WARM, Hanoi, Vietnam

[f] ISARA, rue Baldassini, 69 Lyon, France

[g] Université Savoie Mont Blanc UMR Carrtel, F-73376 Le Bourget du lac

[h] ENSSA Bordeaux Aquitaine, 1 cours du Général De Gaulle F33170 Gradignan Cedx

[i] Université Grenoble Alpes UMR Pacte, 14 bis Avenue Marie Reynoard F 38000 Grenoble

* corresponding author

Email address : dominique.trevisan@inrae.fr (Dominique Trévisan)

Highlights

- We develop OPALE, a suite of programs for the representation and analysis of landscapes in arable crops and grasslands conditions ;
- OPALE allows for efficient evaluation of water and matter outflows (nutrient, suspended matter and fecal bacteria) and leads to usable computed indicators for the assessment of landscape functioning and water-related eco-functionality in various geographical situations.

Abstract

The present article proposes a suite of programs aimed at *(i)* representing landscape organization in relation with the functioning of annual crops or breeding systems, *(ii)* evaluating water movements from biomass and hydrological exchanges, and *(iii)* analyzing the transfer dynamics of nutrients, suspended matter or fecal bacteria based on particle tracking methods. Simulations provided indications about the underlying processes that drive exchanges and sink-source effects operating at the landscape scale. OPALE was tested in three agricultural contexts and biophysical situations. Water flows and flows of associated matters were compared to data recorded at the catchment outlet, and showed the efficiency of the algorithms developed in the generic OPALE libraries. This article describes the underlying hypotheses and the full mathematical framework and procedures used to assess landscape eco-functionality. Several examples are given to illustrate the use of OPALE in landscape reconfiguration prospects (e.g.

influence of landscape composition and structure on plant transpiration, stream flow, erosion, nutrient and organism fluxes in water) for the agroecological transition.

Keywords: farming systems, decision rules, agricultural landscapes, crop management, hydrological processes, agroecology.

1. Introduction

Agroecology is aimed at developing several approaches to solve current agricultural production challenges (Wezel et al., 2009 ; Hatt et al., 2018). It develops field- and territory-level innovations to increase interactions among plant, animal and microorganism communities. As mentioned by Gascuel-Odoux and Magda (2015), a major challenge is not only to promote designs of production systems and crop management methods on an ecological basis, but also to consider innovations at the territorial level. A main challenge is to find ways of defining new farmland organizations to enhance ecological landscape functionalities while considering economic activities, bio-geochemical cycles and biological processes (Poggi et al., 2021). Stakeholders are increasingly concerned by soil management and natural resource protection, as well as by the closure of the water and nutrient cycles, the control of contaminants, etc., as all of them are highly dependent on land use and land cover at the catchment scale.

Agricultural landscapes can be considered as macro-ecosystems resulting from interactions between the human society and biophysical processes. Landscapes constitute *'the mirror of past and present relationships between human beings and their surrounding nature',*

42 Vanier (1995). We considered landscapes as spatial arrangements of features (agricultural fields,
43 urban / forested / semi natural elements like hedges, grass strips, ditches) and flows operating at
44 different time and spatial scales. Some of them are controlled by human activities (flows of
45 energy, fertilizers, farm effluents, flows caused by herd displacements, etc.), others are inherent
46 in the functioning of the eco-biophysical context. Considering the importance of water issues in
47 the context of global change, the ambitions of the agroecological transition (Gascuel-Odoux and
48 Magda, 2015), and landscapes-water quality relationships (Chaplin-Kramer et al., 2016), the
49 present article is focused on landscape eco-functionalities related to water flows (water
50 displacement within landscapes and associated movements of solutes and living or inert
51 suspended matter).

52 The operational assessment of landscape eco-functionalities is aimed at evaluating the
53 links between landscape composition (land uses), structure (spatial arrangement of different land
54 uses), and water flows and nutrient/pollutant flows associated with water movements. It requires
55 the implementation of interdisciplinary approaches. Modeling can offer an adapted framework
56 to analyze and interpret the complexity of landscape macro-ecosystems (Poggi et al., 2021),
57 especially when considering numerous links between decisions, climate, soils and organisms
58 within the critical zone. Landscapes have been the object of several modeling developments,
59 focusing on the design of agricultural territories -see for example MAELIA (Rizzo et al., 2019)- or
60 the interpretation of landscape organizations in terms of water budget and flows -MYDHAS
61 (Moussa et al., 2002)-. To the best of our knowledge, links between these two approaches are
62 sparse. As mentioned by Langhammer et al. (2019) and Zellner et al. (2020), developing generic

63 modeling of the links between human decisions, water needs and water ecosystem functions is
64 central to achieve evaluations of landscapes and elaborate territory prospects in a context of
65 global change.

66 The present article describes OPALE, a tool developed to address the issue of the
67 agroecological transition at the landscape level. The model considers a large set of agricultural
68 production systems and hydrological conditions. It is focused on (*i*) landscape design resulting
69 from farming system parameters and decisions; (*ii*) surface hydrology and biophysical processes.
70 More precisely, the tool includes a set of libraries about the following items:

71 • the design of the landscape occupied by farmland, providing the distribution of
72 crops across farmed fields based on from farming practices and schedules (land use and land
73 cover change model (LULCC));

74 • the modeling of water movements within previous simulated landscapes,
75 considering surface, hypodermical and deep trajectories (water movements within landscapes
76 model (WMWL));

77 • the evaluation of -inert and living- solute and suspended matter transfers
78 associated with water displacements, including N, P, *Escherischia Coli* (EC) and suspended
79 matter (solute and suspended matter transfer (SSMT));

80 • the construction of normalized indicators of landscape functions in order to
81 assess their regulation services.

82

83 A theoretical frame will be first presented to introduce our working hypotheses and our

84 methods. Then, OPALE software architecture will be presented with three different application
85 cases differing in terms of agricultural and hydrological context. They were implemented to assess
86 several issues related to soil conservation, nutrient cycling and surface water eutrophication or
87 the degradation of the bacteriological quality of water resources.
88

89 # 2. Method and Theory

90 ## 2.1. Land use and land cover change (LULCC)

91 The unutilised agricultural area (NUAA) of landscapes (non productive infrastructures,
92 urban areas, forests) is documented by geographical databases (Corine Land Cover, shapes of
93 forested areas)

94 Simulating LULCC in utilised agricultural areas a is somewhat complex because of the
95 diversity of farming systems and associated practices (Thenail et al. ,2009 ; Benoit et al., 2012).
96 Several models working at the plot level (a plot corresponds here to an agricultural parcel: a
97 continuous area of land declared by a farmer, on which a single group of crops is cultivated)
98 concern the organization of annual crop rotations (Dury et al., 2012), but those that enable
99 dealing with livestock or both livestock and crop farms are scarce. One of the difficulties lies in
100 their ability to manage the distribution of technical rules among plots, and their respective
101 contribution to the overall fodder balance for livestock and to commercial benefits for annual
102 crop production.

103 For annual crops, landscapes change every year in relation with crop successions and
104 rotation rules. Taillandier et al. (2012) formulated the choice of crop rotation as a multi-criteria

105 decision problem: for each plot, the farmer chooses a crop rotation, following evaluations at the
106 farm level based on several criteria (financial risk, expected income, workload, farmer's habits).
107 Other works only focus on the crop allocation problem. For example, Martel et al. (2017)
108 formalized it as a constraint satisfaction problem integrating agronomic and crop distribution
109 constraints. Another work using optimization proposes to solve the crop allocation problem by
110 computing the maximum flow of a transition graph of all possible multi-year crop successions
111 (itineraries) permitted by rotation rules (Houet et al., 2014). Then, an optimization process is
112 applied to select the itineraries allowing for the objectives of annual cropping plans (expected
113 surfaces of crop production) to be achieved at the farm level.

114 For livestock and mixed crop-livestock farms, constraints are determined by livestock feed
115 demands. Landscapes are quite stable from one year to the next, as they are not subject to
116 rotation and succession rules. However, the distribution of biomasses varies intra-annually in
117 relation to the grazing and hay-cutting schedule. Landscapes show spatial structures with blocks
118 (assemblages of several plots) of specific uses. We considered three blocks (fig.1): block 1 grouped
119 priority plots for pastures of productive animals (practices P1, HP1, cf. supplementary material
120 S1), permanent or temporary meadows for hay production and late pasture (H3CP1 and H2CP1
121 and HP2), as well as distant pastures for non-productive animals (P2). The area of these blocks
122 depends on the farming system (for example the first block had to provide around 50% of unit
123 forage needs/ha in a milk-round bale system, *versus* 90% for traditionnal systems, cf.
124 supplementary material S1). Several constraints determine the extension and location of these
125 blocks, such as plant growth rates and palatability, distance between livestock sheds and fields,

accessibility, slope and soil conditions (Marie et al., 2016). For example, in case of dairy production, a permanent meadow, according to its slope, its agronomic potential and its distance from the milking parlor, may not be equally assigned to the grazing of dairy cows, hay crops or the grazing of young cattle. Giving that livestock headcount cannot be easily changed in livestock systems, landscape construction was modeled with reference to cascade rules and supply-demand constraints, where pasture for productive animal are the priority, followed by crops and hay crops productions and finally pasture for heifers or lots of non productive animals for the remaining surfaces (Josselin et al., 1999). As the drivers of the distribution of activities of a crop farm and a livestock farm differ greatly, we did not use the same approach to represent the landscape design.

For crops farms (including vegetable production), we chose an algorithm similar to the one proposed by Houet et al. (2014) where the spatial distribution of crops depends on an optimization process based on maximal flow computations. In this representation, activities are constraint by cropping plans and rules related to permitted of forbidden crop rotations (Figure 1), with the following hypothesis: (*i*) in the case of vegetable production with crops requiring regular/daily intervention (seeding/planting, harvesting/packaging), priority blocks nearby working sheds must be first allocated before implementing maximum flow computations; (*ii*) crop system landscapes do not change according to seasonal climate changes as farmers can adjust irrigation schedules or change the final commercialization of the harvested products depending on the way meteorological conditions evolve; (*iii*) all the plots concerned by the maximum flow computation are considered to be unconstrained by edaphic (humidity, stoniness, etc.),

topographical (slope) or cadastral conditions. In the event that one or several plots cannot be used for annual crops, their dominant use must be indicated in the geographical database describing the NUAA.

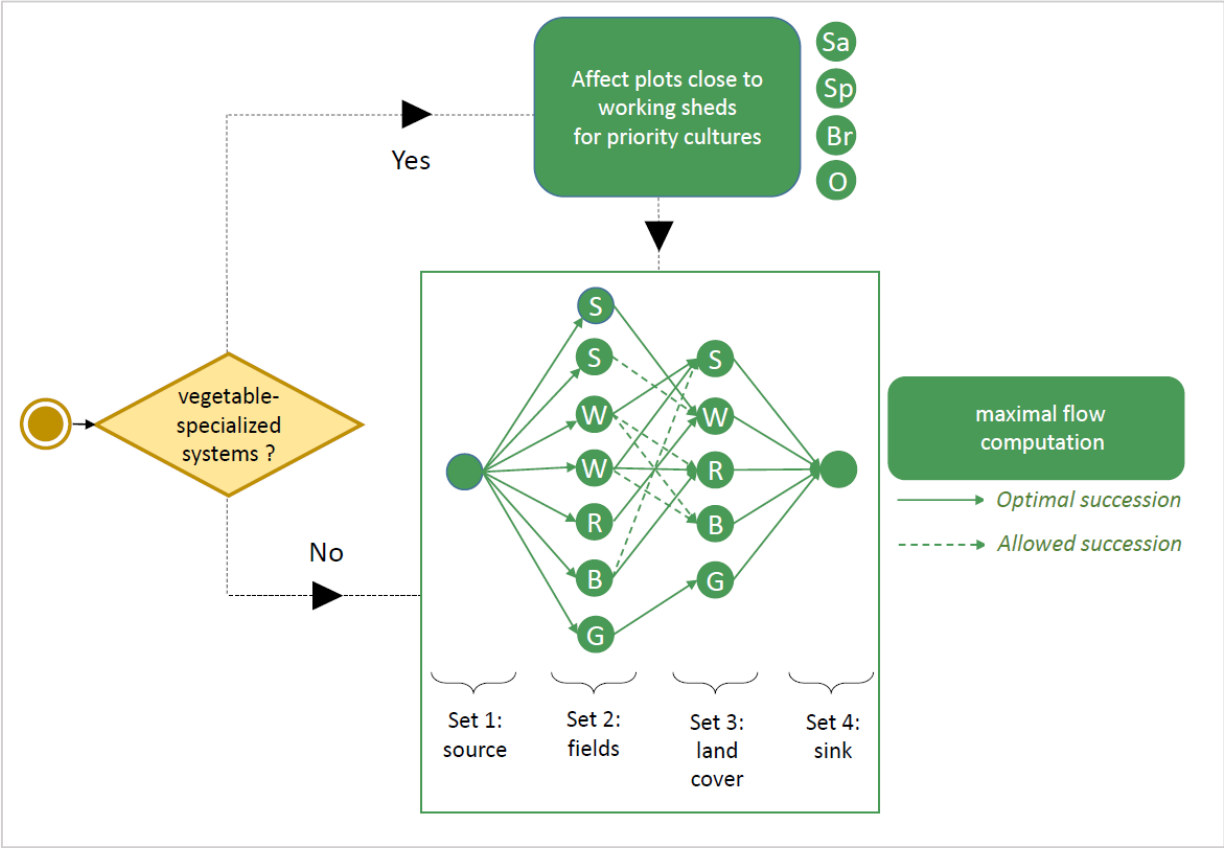

Figure 1: Diagram of the LULCC model for crop systems. For non-priority crops possibly remote from working sheds, a maximum flow computation was performed, extracted from Houet et al. (2014). W-Wheat; B-Barley; R-Rapeseed; S-Sunflower; G-Grassland; S-Salad; Sp-Spinach; Br-Beetroot; O: Onion. For the sake of simplicity, this diagram represents an example of a two-year succession of crops (in practice, the number of crop successions can be defined by the user). Arrows between Set1-Set2 and Set2-Set3 represent graph edges with a capacity equal to field surfaces; between set3-Set4, edges with a capacity equal to the total surface of a given farm. An

158 optimization process selected an itinerary between Set1 and Set4 across a total area similar to
159 the farm's cropping objectives.
160
161 The maximum flow was computed using the classic Edmonds-Karp max flow algorithm
162 (Edmonds and Karp, 1972). As this algorithm is stochastic, different solutions of spatial crop
163 allocation can be obtained between two executions depending on random choices for the
164 construction of graph-edges. Unlike Taillandier et al. (2012), labor tasks were not explicitly
165 evaluated, but plowing, sowing and hoeing dates were stochastically distributed in the computed
166 crop successions to generate "noise" in calendars.
167 For livestock farms (Figure 2), we implemented stepwise computations controlling the
168 adequacy between plot supply and the priorities for pasture and forage demands, as proposed
169 by Marie et al. (2016). Considering farming systems and livestock heads, we determined the
170 forage needs and allocated them to farmlands, following priorities and surface ratios of forage
171 practices (intensive or extensive meadows and pastures), cf. supplementary material S1. We
172 considered that the extent of spatial blocks could change under unfavorable climatic situations
173 because livestock feeding is priority over the constitution of forage stocks. Landscapes and the
174 dynamics of grass biomass were therefore modified following seasonal climatic evolution in
175 accordance with priority rules for livestock needs.

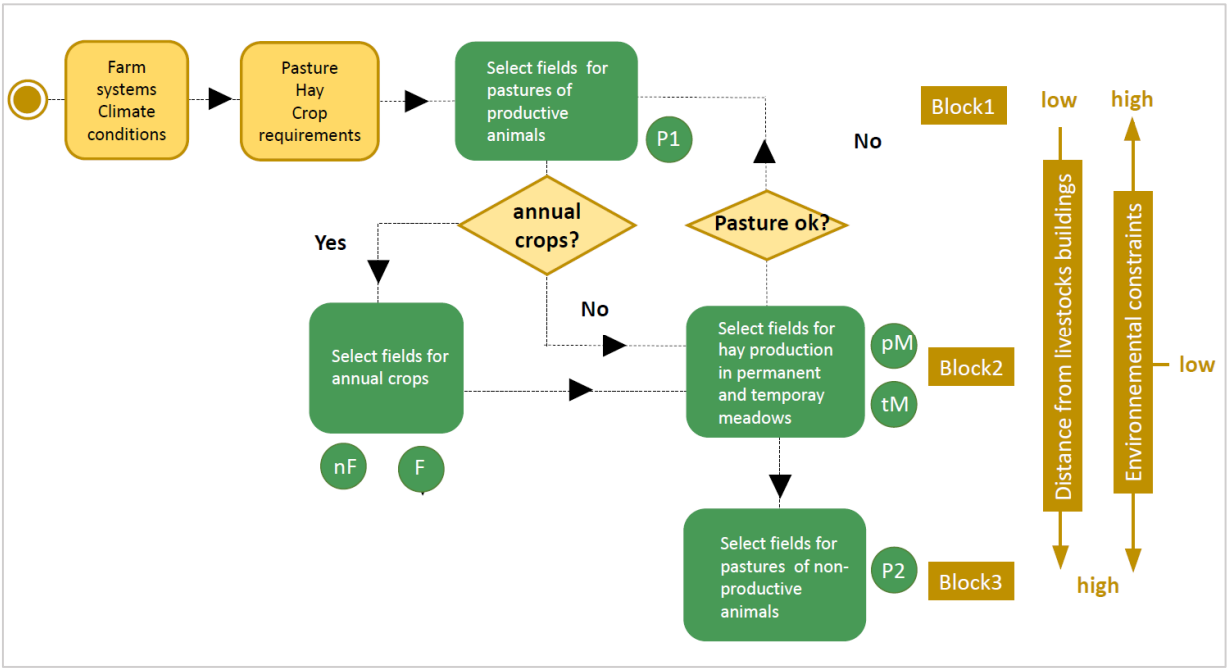

Figure 2: Diagram of the LULCC model for livestock systems. nF-non forage crops; F-forage crops; P1-first-priority pastures for productive animals; pM-permanent meadows; tM-temporary meadows; P2-second-priority meadows for non productive animals. Three blocks of fields composed the farm landscape, in relation with distance to livestock sheds and environmental constraints (slope and soil moisture). A step computation scheme selected the available fields for the crop requirements of the farm systems and several climatic conditions. Pasture requirements for productive animals were computed iteratively by adding P1 surfaces and late pastures following hay cuts.

The time step for the simulations of livestock or crop systems is one day, and the time span of the simulation is fixed by the user (one year is the minimum required to buid a landscape over the seasons, much longer in crop sytems to evaluate landscape evolution according to successions).

2.2. Water movements within landscapes (WMWL)

189 Modeling water movements requires implementing distributed approaches in which a
190 computational domain is defined by the watershed boundaries (a watershed is a land area that
191 channels rainfall and snowmelt to rivers and to an outflow point), generally represented by
192 square grid meshes where each individual cell (defined as a sqare area of a dimension fixed by
193 the pixel dimension of the digital elevation model) is the object of water balance. Computations
194 may use simultaneous or sequential approaches.

195 In the simultaneous approach, implicit digital schemes can be performed to solve partial
196 differential matrix equations, considering all flows and local processes of the computational
197 domain, as in MODFLOW (Harbaugh, 2005). Such an implementation is no straightforward task.
198 As an example, boundary conditions must be defined for domains where the deepest geological
199 structures and their links with the hydrological network are generally unknown or poorly known.
200 Also, the stability of the solution of the matrix equations is unsure because it depends on the
201 configuration of the digital schemes.

202 To overcome these difficulties, the sequential approach considers cell balance solved
203 explicitly by cascade schemes, from up-slopes to the watershed outlet, Kiesel et al. (2013). In
204 addition, all the processes that control soil moisture (e.g., evapotranspiration, percolation) are
205 evaluated successively, in the same way as in the distributed SMDR model (Gérard-Marchant et
206 al., 2006), or in the semi distributed SWAT model (Arnold and Fohrer, 2005). We chose this
207 approach although it does not represent hydrodynamic processes simultaneously. First, errors
208 are restrained when time-step computations are shortened (Trevisan and Periáñez, 2016);
209 second, there are several operational gains: (*i*) the deepest domain can be represented by black-

box representations, (*ii*) equations are formal, giving an eprouved ability to provide evaluations of time-varying land management practices (Me et al, 2018) ; (*iii*) no solver configuration is required.

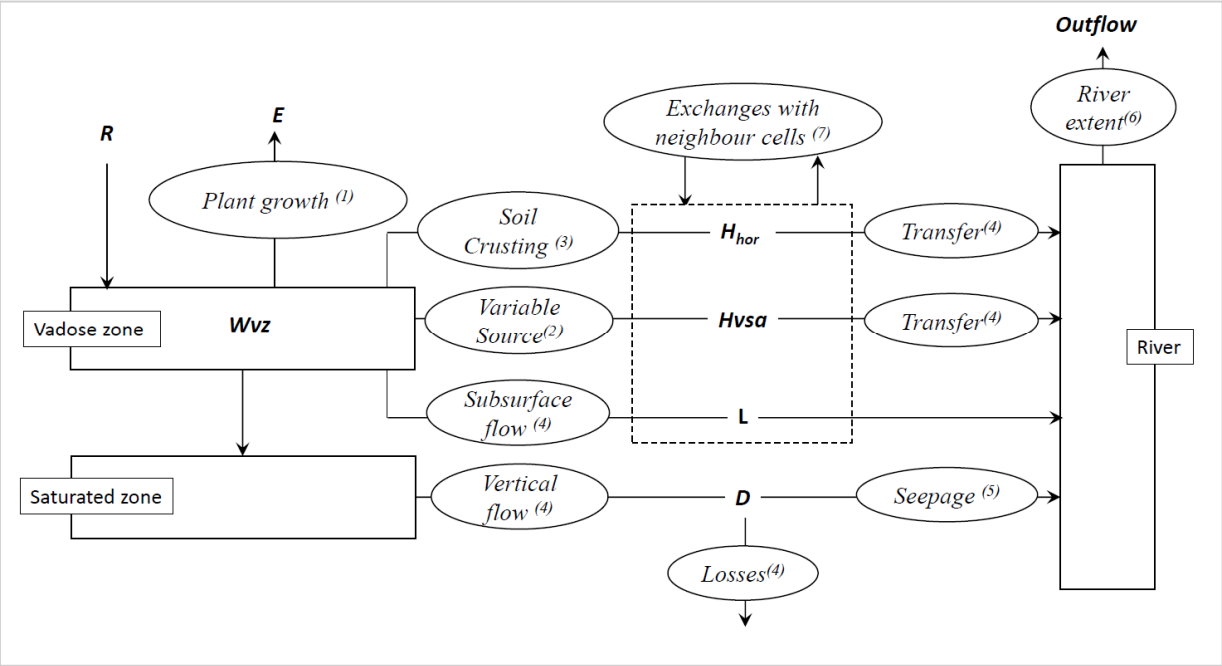

Figure 3: Computation algorithm and parameterization of the water flow model. Rectangles represent water stores, ellipses processes. Exponent values in parentheses refer to the following works: *(1) Gérard-Marchant et al. (2006); (2) Obled and Zin (2004); (3) Cerdan et al. (2002); (4) Arnold and Fohrer(2005) ; (5) Lellay (2006); (6) Gurnell (1978); (7) Tarboton (1997).* Refer to the text for comments.

Two soil volumes were considered in the WMWL model: (i) the vadose zone in the topsoil, delimited by root depth, overlying (ii) the saturated zone (figure 3). The general water balance for extended hydrodynamic situations was:

$$\frac{dW_{vz}}{dt} = R - E + L + H_{vsa} + H_{hor} + H_{imp} - D, \quad (1)$$

where W_{vz} is the water store in the vadose zone [mm], dt the time interval [d], and the following all expressed in [mm.d^{-1}]: R rainfall, E evapotranspiration, D vertical drainage, L the lateral movements of water (sub-surface flows), H_{vsa} overland flow generated by soil saturation (variable source area (runoff), H_{hor} hortonian runoff, H_{imp} overland flow from impermeabilized urban areas, and D vertical drainage. L, H_{vas}, H_{hor} and H_{imp} net values can be positive or negative depending on whether water flows are coming from up-slope cells or directed to down-slope cells, respectively. The processes controlling the water balance equation are summarized in Figure 3.

We accounted for a large diversity of hydrodynamic processes to extend the applicability of the WMWL model to generic situations.

• Biomass dynamics, root depth and evapotranspiration flows were computed for vegetables, crops and pastures by the generalized plant growth model (Gérard-Marchant et al., 2006), detailed in Appendix A, §7.1. The model is based on a computation of cumulative degree-days. Several thresholds were considered, accounting for plant growth rates, practices and farming schedules (seeding, cuts, etc.), all of them tabulated from the LULCC model outputs;

• We introduced first-order kinetics to describe water table behavior (Arnold and Fohrer, 2005 ; Lellay, 2006). The seepage of the water table into the river network was evaluated from a transfer function applied during a restitution period (Hingray et al., 2009). In this representation, one of the major issues (Sarrazin, 2012) is the capacity of the model to reproduce the hydrologically active areas of watersheds (zones where groundwater tables can effectively

seep into the river network). Following Gurnell (1978), we considered that the representation of a river network dynamics accounted for temporary drying out of the river network, and calculated the number of river segments where seepage was effective;

• Hypodermic water movement along slopes where topsoils are bounded by restricting layers or low-permeability layers can favor the rising of sub-surface water tables over the soil surface in thalweg and down-slope conditions (Obled and Zin, 2004 ; Gérard-Marchant et al., 2006). For this reason, the Variable Source Area hydrology concept (Dunne et al., 1975) was integrated in the WMWL computing scheme;

• Soil surface crusting is a main determinant of hortonian runoff. Process-based models –e.g., see Jetten et al. (1998) - were developed to estimate hortonian runoff flows from hydrodynamic properties of soil surface crusts. Their applicability to agricultural contexts where the crusting dynamics is driven by farming practices and plant biomass development is challenging (Takken et al., 1999). To avoid over-parameterization, we implemented expert-based rules from the STREAM model (Cerdan et al., 2002) to focus on the dominant drivers of crusting;

• Following Kiesel et al., (2013), we implemented a cascading computational scheme to evaluate water flows along slopes, in which water balance was calculated for successive cells sorted by decreasing elevation and increasing index of topographic accumulation (Schwanghart and Kuhn, 2010).

WMWL equations are fully described in Appendix A.

2.3. Solute and suspended matter transfers (SSMTs).

265 The SSMT model calculates transfer functions to provide standardized evaluations of
266 landscape functioning and help end-users in the comparison of landscape configurations and
267 structures. Transfer functions correspond to a density of mass-transfer rate of compounds
268 originating from transient stores, often described by exponential or power-law distributions
269 (Haggerty et al., 2002). We calculated surface and subsurface transfer functions (*SSTFs)* for
270 surface and subsurface flows by applying particle-tracking methods, considered as a key
271 technology for assessing the diversity of displaced matters (Chenouard et al., 2014). Here,
272 particles represent a solute mass of nutrients in solution, SM or EC numbers.

273 To assess landscape functioning during critical periods and save computational time, *SSTF*
274 calculations were restricted to ''transfer periods'' ($t - \tau_f, \ldots, t$), where τ_f is the transfer
275 duration (days), following a daily meteorological event of interest (DMEI) starting at date $t - \tau_f$.
276 DMEIs are events representative of typical soil moisture conditions and biomass development,
277 e.g., low-water periods or fall high-flow recovery. During the transfer period, the SSMT module
278 counts the number of particles that reach the watershed outlet as a function of water trajectories
279 computed by the WMWL model and sink-source determinism. Water trajectories and particle
280 displacements can be interrupted on cells where the soil moisture balance does not exceed
281 saturation thresholds. During the transfer period, we restricted water exchanges with the
282 atmosphere to evapotranspiration flows (rainfall was set to 0) to only account for particle
283 displacements resulting from the landscape draining and water redistribution dynamics produced
284 by DMEIs.

285 Particle tracking was based on previous schemes accounting for pollutant build-up, wash-

286 off and transport processes (Jiang et al., 2019). During the transfer period, for each τ days of the
287 interval $(0, \dots, \tau_f)$, we considered the $s_k(t-\tau)$ build-up stocks located on the k cells of the
288 computational domain, each of them affected by wash-off rates $w_k(t-\tau)$ transferred to the
289 outlet with associated $p_k(\tau)$ transfer probabilities. Based on Trévisan et al. (2019), the amount
290 of particles produced by a DMEI was given by:

291 $$\sum_0^{\tau_f} q(\tau) = \sum_0^{\tau_f} \sum_1^k s_k(t-\tau) w_k(t-\tau) p_k(\tau). \quad (2)$$

292 For surface and subsurface flows, transfer delays are generally short, in the range of
293 several days or one/two weeks (Dorioz et al., 1989). Consequently, the following build-up stocks
294 $s_k(t-\tau_f, \dots, t)$ and wash-off 3D matrices $w_k(t-\tau_f, \dots, t)$ were computed for $\tau_f =$ 15 days.
295 Two indicators of underlying processes driving exchanges and sink-source effects operating at the
296 landscape scale were evaluated by SSMT outputs. First, the DMEI-*SSTF* distribution obtained by
297 particle counting at the catchment outlet:

298 $$P(1), \dots, P(\tau_f) = \frac{q(\tau)}{\sum_0^{\tau_f} q(\tau)}. \quad (3)$$

299 Second, $\eta(t-\tau_f)$, the landscape delivery ratio associated to the DMEI started at $(t-\tau_f)$:

300 $$\eta(t-\tau_f) = \frac{\sum_0^{\tau_f} q(\tau)}{\sum_1^k s_k(t-\tau_f) w_k(t-\tau_f)} , \quad (4)$$

301 varying from 0 for systems in which no matter flows out of the landscape to 1 in opposite
302 conditions. *SSTF* and $\eta(t-\tau_f)$ provided by particle counting were catchment-scaled and DMEIs
303 single-event-dependent representations of landscape functioning. The SSMT equations of particle
304 behavior driving $s_k(t-\tau)$, $w_k(t-\tau)$ and $q(\tau)$ values are given in Appendix B.

305 Deeper transfer delays were greater than previously, in the range of several months

(Hingray et al., 2009). As the groundwater table was represented by a black-box analysis, particle counting was not fitted. The corresponding groundwater transfer function (*GTF*) was given by $P(1),\ldots,P(\tau_s)=\tau_s^{-\lambda+R}$, with λ a WMWL power-law parameter for deep water transfer (Appendix A), τ_s the duration of the seepage period, and R a retardation factor accounting for sink effects (Holzbecher, 2012) equal to 0 in case of N transfer (no sinks outside the vadose zone). *GTF* were catchment-scaled and generic-event scaled representations of landscape functioning.

2.4. Model validation

2.4.1. LULCC and WMWL modeling

We evaluated the deviation between the farmers' cropping plans and the simulated plans through the absolute deviation $AD=\frac{\sum_{i=1}^{n}|\hat{X}_i-X_i|}{\sum_{i=1}^{n}\hat{X}_i}$, where $1\ldots n$ is the set of possible land uses, $\hat{X}_i$ the sum of areas of land use i expected by the cropping plan, and X_i the corresponding simulated sum. River outflows summing all water components computed by the WMWL model were confronted to observed values trough the Nash Sutcliffe coefficient (Wallach et al., 2013).

2.4.2. Particle tracking and SSMT modeling

The amount $q(t)$ of particles reaching the outlet depends on delayed flows that affect the number of particles $m_k(t-\tau)$ produced in each cell of the computational domain and available for water transfer:

$$m_k(t-\tau)=s_k(t-\tau)w_k(t-\tau). \quad (5)$$

We can write:

$$q(t) = \sum_1^k \int_0^{\tau_f} m_k(t-\tau) p_k(\tau) d\tau = \sum_1^k m_k(t) * p_k(\tau), \quad (6)$$

where the asterisk represents the convolution product and $p_k(\tau)$ the transfer probabilities generated by DEMIs representative of hydro-agrosystem conditions over the transfer period.

The individual particle behaviors and trajectories of surface and subsurface transfers cannot be measured directly. To compare SSMT results with observed values, we introduced delivery ratios (eq. 4), produced stocks m_k (eq.5) and *SSFT* $P(\tau)$ (eq. 3) values into a lumped formulation of particle flows $q_L(t)$ equivalent to $\sum_1^{\tau_f} q(\tau)$, the SSMT outflows (Appendix C):

$$q_L(t) = \eta(t-\tau_f) \sum_1^k m_k(t) * P(\tau). \quad (7)$$

In case of finite built-up stocks, the production function is lowered by previous outflows, with minimum values fixed to 0:

$$\sum_1^k m_k(t) = \sum_1^k s_k(t) w_k(t) - q_L(t-1) \quad (8)$$

For nutrient and EC stocks, $s_k(t)$ were obtained by updating the balance $s_k(t) = s_k(t-1) - \gamma s_k(t-1)$, where γ accounts for plant assimilation/mineralization/de-nitrification/mortality. At the beginning of the simulation (t_0) or for each period of fertilizer supply or manure disposal, initial $s_k(t_0)$ values were defined considering fertilization supplies or residual stocks of land uses (supplementary material S2). For SM, $s_k(t)$ depended on the crusting dynamics (Appendix B).

Solute matter outflows from deep water table seepage were calculated by eq. 7, where

347 the distribution $P(\tau)$ is given by the *GTF* (cf. paragraph 2.3) and $\eta(t-\tau_f)=1$.

348 Lumped-computed N, total P and soluble P, EC and SM outflows were confronted in
349 separate worksheets to observed values, following Trévisan (2019). A unit conversion factor u
350 was evaluated by minimizing the objective function $[q^{obs}(t)-uq_L(t)]^2$ between observed
351 q^{obs} and calculated q_L values of matter outflows.

352

353 # 3. Software architecture

354 WMWL and OPALE GUIs (figure 4) were implemented in the MATLAB environment, while
355 the LULCC and SSMT programs (figure 5) were implemented with the GAMA platform (Taillandier
356 et al., 2019). The OPALE GUI allows users to select libraries, implement IOF writing/reading and
357 parameterize commands in the two environments and SAGA geographical treatment
358 (http://www.saga-gis.org). OPALE executable for the Windows-64 bit environment, source codes
359 and documentation are available at github[1]. All programs were run on a computer with a CPU
360 IntelCore(R) i7 and 32 Go RAM.

[1] https://github.com/TipTop-PSDR/OPALE.git

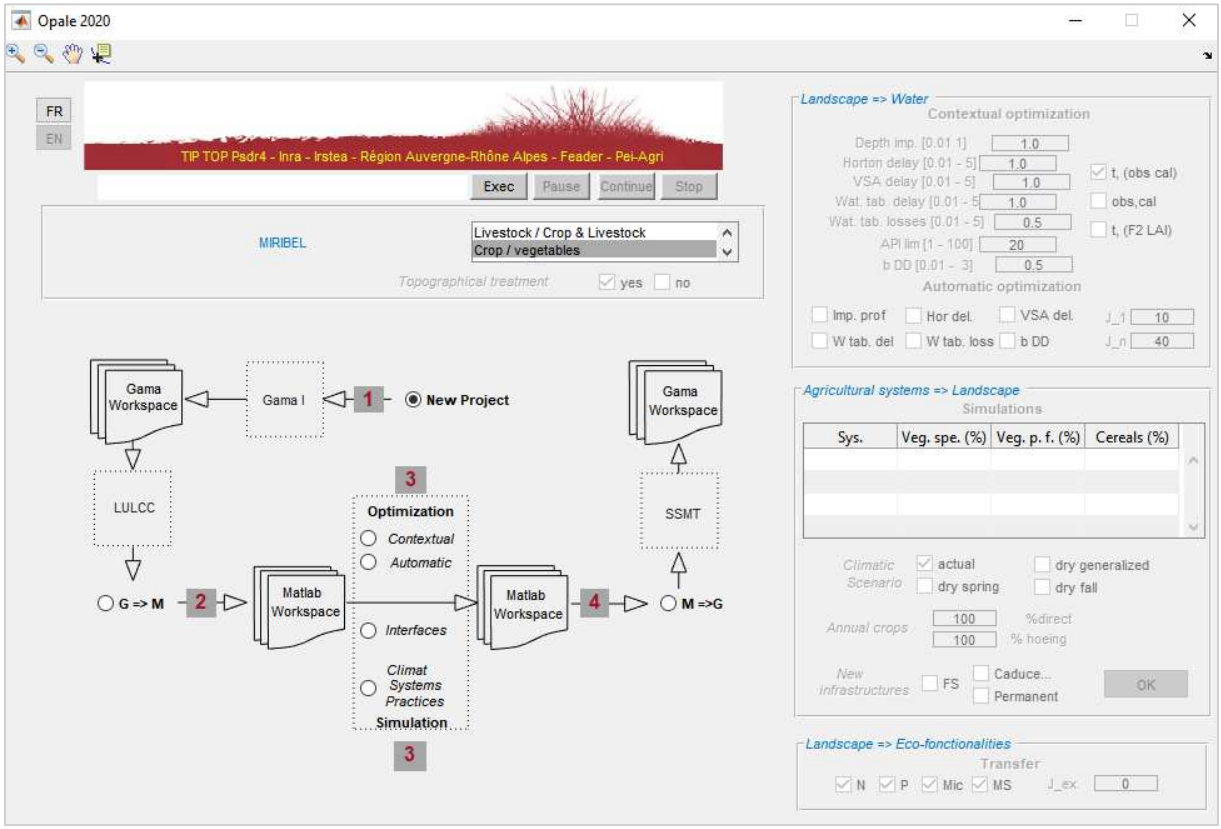

Figure 4: OPALE GUI.

At the center of the OPALE GUI a workflow scheme organizes the workflow steps for landscape assessment. The workflow scheme differs depending on the selected production systems (from the listbox items - Livestocks / Crops & Livestock or Crop / vegetables-).

At step 1, the 'New project' button and a subsequent 'Exec'-clic allows reading input files. Then, it opens the GAMA GUI where users can launch an initialization program, linking together geographical information (soils, hydrological network, fields, farm systems, etc., as described in supplementary material S3). The computational mesh is also defined here, with the sizes of the square grids based on the resolution of the digital elevation model.

Then, the LULCC program is opened, and performs maximum flow or step computation

schemes depending on the selected production systems. Configuring decision rules for crop successions and distance priorities between farms and practices is allowed. LULCC outputs are agricultural landscape structures (i.e. an assemblage of different agricultural plots) and landscape infrastructures (e.g. hedges, filter strips, non-productive areas), as referenced by grids where their proportion area in the cells of the computational mesh are calculated to limit topological representation biases for the following WMWL calculations.

The 'G=> M' button (Step 2) builds matrices for the Matlab environment and performs plant development and topography calculations to build the cascade scheme for sequential water flow balances along slopes.

The Step 3 top buttons open the WMWL model for optimization. WMWL optimization can be done contextually based on soil and hydro-system properties, or automatically with the *lsqcurvefit* tool in Matlab. All calculations up to this stage provide a baseline on the current landscape.

The Step 3 bottom buttons open simulation purposes, and build new matrices that can be compared to the current landscape. If the user needs to analyze production system changes, the workflow differs depending on farming conditions. For crop/vegetable systems (crop distribution determined by random selections in the LULCC model), forward planning of farming systems is implemented by modifying the crop areas of the first year of the crop succession in order to follow the initial patterns of crop distributions. The aim is to avoid repeated simulations to obtain converging agent-based model simulations outputs that are commonly done to compare present and future territories (Grillot et al, 2018). The price to pay is that only the first year of the crop

succession of current and future landscapes can be compared. We implemented such modifications within the Matlab environment, where the first year of the current landscape matrices of crop allocation are modified according to the expected proportions of crop groups indicated by the user in the agricultural-system-landscape panel. To do this, we applied an algorithm in which parcels are progressively assigned to new expected productions until the user's constraints are met. As breeding landscapes are not constrained by random choices of potential crop successions but by priority schemes, modifications of farming systems and climatic conditions have to be calculated by re-launching the LULCC model on an annual or pluriannual basis in which each new farming objective indicated in the agricultural system-landscape panel is evaluated in terms of priority practices and field availability.

Step 4 allows opening an M=>G library to configure the s_k build-up matrices for Gama SSMT modeling.

On the right side of the OPALE GUI, three panels are enabled/disabled depending on the workflow selection step. The 'Landscape => Water' panel contains several dialog boxes for WMWL parameters (k_m, c_1, c_2, c_3, λ, b, i_{max}, see Appendix A) and check-box options to configure WMWL output plots (when the 'obs, cal' check-box is selected, the Nash Sutcliffe coefficient (Wallach et al., 2013) is computed to compare observed or calculated river flow outputs) or to select parameters to be optimized by the *lsqcurvefit* program. Optimization processes can be paused for plot-zooming and inspection (from the upper tool bar) or to analyze the contributions of water components to river outflows or select DMEI dates. The 'Agricultural system => Landscape panel' allows configuring the proportions of the farming systems, as well

414 as climatic conditions, farming practices or infrastructure distribution (several choices are
415 possible, with filter strips or hedgerows of deciduous of perennial tree species). With the
416 'Interface' button, the program interacts with SAGA libraries to re-calculate the proportions of
417 the infrastructures in the computational meshes. Finally, with step 4, the 'Landscapes => Eco-
418 functionality' panel allows evaluating the transfer functions *SSTF* and the nature of the particle
419 matter to be treated in SSMT.
420

421 4. Examples of applications

422 4.1. Catchment description and monitoring

423 OPALE was tested in three different territories in terms of farming systems and
424 geographical conditions. Site properties are given in table 1.
425

Site	Area (ha)	Localization wgs84	Agricultural systems	Geography
Miribel	1132	lat.: 45°.853 lon.: 4°.943	Annual crops Vegetables	altitude: 300 m geology: loess main soils: haplic lixisols main use: agriculture
Autrans	1965	lat.: 45°.107 lon.: 5°.532	Livestock Annual crops	altitude: 1,000 m geology: lacustrine deposits main soil: cambisols main use: agriculture-tourism

Aiguebelette	2700	lat.: 45°.572 lon.: 5°.799	Livestock	altitude: 500 m geology: sandstones, glacial deposits main soils: gleysols main use: agriculture-periurban

Table 1: Study sites. Summary of agricultural and geographical conditions. The main soil types are referenced from the World Reference Base for Soil Resources (2014).

Geographical inputs are detailed in supplementary materials S3. Miribel catchment was mainly concerned by hortonian overland flows from annual crops, including fine silt texture conditions and a high sensitivity to soil surface crusting (Lepilleur, 2017). Due to the low permeability of lacustrine deposits preventing deep water percolation, Autran catchment was subject to soil moisture saturation of variable source areas causing frequent surface runoff (Petitqueux, 2017). On the contrary, Aiguebelette tertiary sandstone was favorable to high soil permeability, and water percolation was predominant (Pezet, 2014). Poulenard et al. (2009) studied a catchment nearby Aiguebelette sharing the same geographical context and showed that matter from riverbank erosion was predominant in suspended matter flows and that livestock played a role too. These authors observed that the relative contributions of topsoils and river bank sediments were seasonal, with an increase of the topsoil contribution during spring and summer pastures and a decrease in late fall and winter, in relation with the access of livestock to the river network.

Stakeholders are concerned by erosion, soil protection and mud flows in Miribel, nutrient

losses and eutrophication of surface waters in Aiguebelette, and bacteriological water quality in Autrans.

Stream flows were monitored using weirs placed at the catchment outlets. Water samples were collected in 2016 and 2017 by automatic samplers programmed for weekly flow-weighted composite sampling. In Miribel, the Nephelometric Turbidity Unit (NTU) was monitored with an OBS300 Campbell Scientific probe for SM flow evaluation. In Aiguebelette, SM, soluble reactive phosphorus (SRP), total phosphorus (TP) and nitrates were analyzed by standard colorimetric methods (AFNOR, 1990). In Autrans, instantaneous water samples were collected manually and sent within 24h to the laboratory for EC enumeration, following standard protocols ISO 9308-2 for water bacteriological quality assessment. In addition, to differentiate between the proportions of human and bovine contamination, water sub-samples were treated to quantify HF183 and Rum2Bac bacteroidales markers, following Mauffret et al. (2012).

4.2. Model parameterization

Table 2 gives parameter values for the WMWL and SSMT models. We evaluated the parameters of the WMWL model (k_m, c_1, c_2, c_3, λ, b, i_{max}), following the *lsqcurvefit* automatic optimization module or by referencing contextual values from expert estimation.

Parameter	Definition	Value	Source
T_b, $DD_{1..max}$	temperature thresholds (§ 7.1)	reference values	SMDR (2013)
k_m	bottom K_{sat} ratio (eq. 15) [-]	M.: 1.0; Au.: 0.8; Ai.: 1.0	C. op.
c_1	deep aquifer losses (eq.20)	M.: 0.88; Au.: 10; Ai.: 1.3	A. op.

	[d^{-1}]		
c_2	overland hortonian delay (eq.21) [d^{-1}]	M.: 5.0; Au.: 5.0; Ai.: 5.0	C. op.
c_3	overland saturation delay (eq.21) [d^{-1}]	M.: 1.0; Au.: 0.01; Ai.: 1.0	A. op.
λ	groundwater delay (eq.22) [d]	M.: 2.5; Au.: 1.5; Ai.: 1.4	A. op.
b	river shape form (eq.23) [-]	M.: 2.5; Au.: 2; Ai.: 2.5	A. op.
i_{max}	maximum API bound (eq.24) [mm]	M.: 80; Au.: 100; Ai.: 80	C. op.
n and α	Van Genuchten's eq. (§ 7.5) [-]	M.: $n = 1.25,\ \alpha = 0.08$ Au.: $n = 1.52,\ \alpha = 0.02$ Ai.: $n = 1.25,\ \alpha = 0.05$	Wosten et al. (1999)
I	mean rainfall intensity (eq. 18) [$mm.h^{-1}$]	20	Evrard et al. (2009)
c_{F2}	crust dynamics parameter (eq.19) [-]	reference values S4	Lepilleur (2017)
s_k	crop P and N requirements (§ 8.1) [U of P or $N.d^{-1}$]	reference values S2	COMIFER (2013)
δ_P	particulate material wash-off (§ 8.2) [$m^3.s^{-1}$]	4.10^{-5}	Lafforgues (1977)
δ_s	solute material wash-off (§ 8.2) [$m^3.s^{-1}$]	0.3	Burns (1974)
n_a	daily assimilation rate (§ 8.3) [U of $N.d^{-1}$]	reference values S2	COMIFER (2013)
K_d	EC daily mortality coefficient (§ 8.3) [d^{-1}]	reference values S2	Trévisan et al. (2002)
d	daily denitrification (§ 8.3) [U of $N.d^{-1}$]	0.05	Nicolardot et al. (1996)
r	SM build-up source (§ 8.3) [-]	1.5	Mamedov et al. (2016)
β	retention parameter (§ 8.3) [m^{-1}]	$\beta_{SM} = 0.25,\ \beta_{PT} = 0.35$	Trévisan et al. (2002)
θ	source parameter (§ 8.3) [-]	$\theta = 1.5$	Trévisan et al. (2002)

462

Table 2: Parameter values (M.: Miribel; Au.: Autrans; Ai.: Aiguebelette; C. op.: Contextual optimization; A. op.: automatic optimization). S2 : supplementary material 2 ; S4 : supplementary material 4.

Doing so and considering the respective soil conditions, the bottom permeability ratio k_m was high in Miribel and Aiguebelette but low in Autrans. Horton store emptying was considered rapid, and a maximum c_2 value was thus retained. The saturation overflow emptying value c_3 was lower, considering potential retardation effects due to variable extension of source areas. All SSMT parameters were predefined (δ, a_k, d_k, k_d, r_k, e_k), referenced from available data given in table 2, as well as those proposed in the LULCC model (supplementary material S1 parameters), although a few decision variables can be redefined from the GAMA GUI to account for local organization and decision rules (fig. 5).

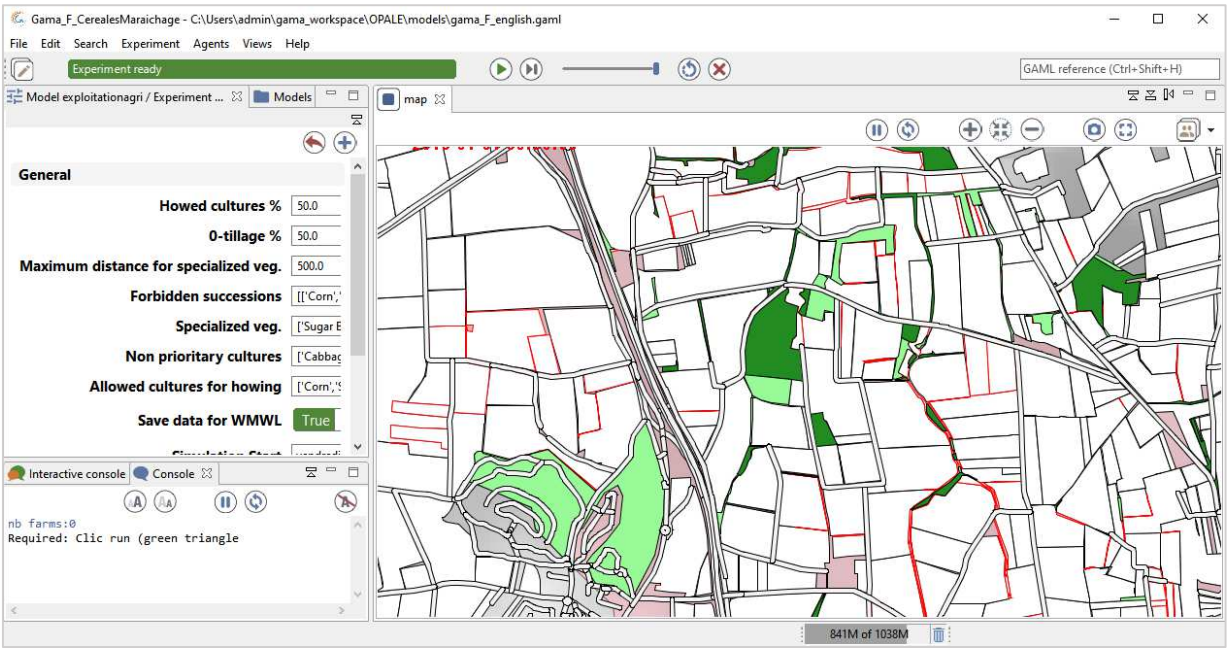

Figure 5: GAMA GUI. A button and list-box panel allows the user to define parameter values and conditions for generating landscapes and controlling the output configuration.

4.3 Landscape reconfiguration prospects

Landscape reconfigurations were simulated to evaluate several agro-ecological transition schemes aimed at valorizing landscape ecofunctionnalities and controlling water cycle and quality. The values of the parameters were fixed following those indicated in table 2, giving reference states R to which the effects of landscape reconfigurations S were compared. We evaluated the efficiency E_f of the reconfigurations by $E_f = 1 - \frac{\sum_1^k \sum_0^{\tau_f} q_S(\tau)}{\sum_1^k \sum_0^{\tau_f} q_R(\tau)}$ (low values correspond to low efficiency) where k, q_S and q_R are the number of DMEI, and the counts of particle outflow generated by the reconfigurated landscape and of the reference state, respectively.

4.3.1. Farming system evolutions and grassland landscape reshaping to control vole overgrowths and bacteriological water quality degradation

Specialized livestock breeding territories can be associated with faecal contamination of water but also with grassland vole overgrowths, in relation with low landscape heterogeneities, the increasing number of permanent meadows, the lack of disturbing activities (plowing) or natural barriers (paths, banks) for rodent populations, as well as the regression of natural refuges (hedges, forested patches) for terrestrial and aerial predators (Halliez et al, 2015). The following changes were tested on *E. coli* flows in the Autrans area: (i) modification of farming systems to increase the area of plowed parcels (two cases were evaluated with introductions of 10ha and 25ha of spring barley in cereals-milk round-bale systems, corresponding to 1.5 and 3.8 % of

497 additionnal plowed surface in the watershed area, respectively); (ii) implementation of hedges
498 (5m wide, considered equivalent to a caduceous forested area) following 5 modalities: 10 km long
499 along a preferential east-west direction; 10 km along a north-south direction; 10 km EW and 10
500 km NS; 20 km NS; 20 km NS and 10 km EW).

501 **4.3.2. Changes in farming systems and agricultural practices, and implementation of grass filter**
502 **strips to control soil erosion and suspended matter flows**

503 Industrial vegetable production is often associated with soil compaction and severe runoff and
504 erosion events (Lepilleur, 2017). We evaluated the effects of changes in the distribution of
505 farming systems on SM with a 10% increase of annual crop systems in the Miribel area. In
506 addition, we tested the generalization of hoeing on row crops and the implementation of 0.2, 0.4,
507 3.4, 3.8, 22, 42 and 96 ha of grass filter strips (these latter filters were first positionned on critical
508 source aeras selected by vizualizing displacements of SM particle clouds – cf. fig.11 – and
509 thereafter generalized to the catchment along the drainage network).

510 **4.3.3. Water management**

511 As a consequence of periurbanization in the Aiguebelette area, stakeholders are confronted with
512 the extension of the artificial hydrological network aimed at draining humid areas. We tested the
513 effect of river network reshaping on SRP loads by adding 1296m of open drain length to the 4262
514 m of the present hydrological network in a sub-catchment (137 ha) of the studied area (2700 ha).

515 ## 4.4. Discussed results

516 **4.4.1. LULCC modeling**

517 For crop/vegetable landscapes, the AD ratio between expected crop surfaces and

518 calculated crop surfaces differed depending on the farming systems (fig. 6). Mean values were
519 centered on 1, showing the ability of the LULCC model to construct reliable landscapes according
520 to the farm production objectives. For annual crops and mixed systems, the deviation from the
521 mean was low. However, it was greater for specialized vegetable systems, as a great number of
522 vegetable species can be introduced in crop successions depending on the evolution of the
523 market demand.

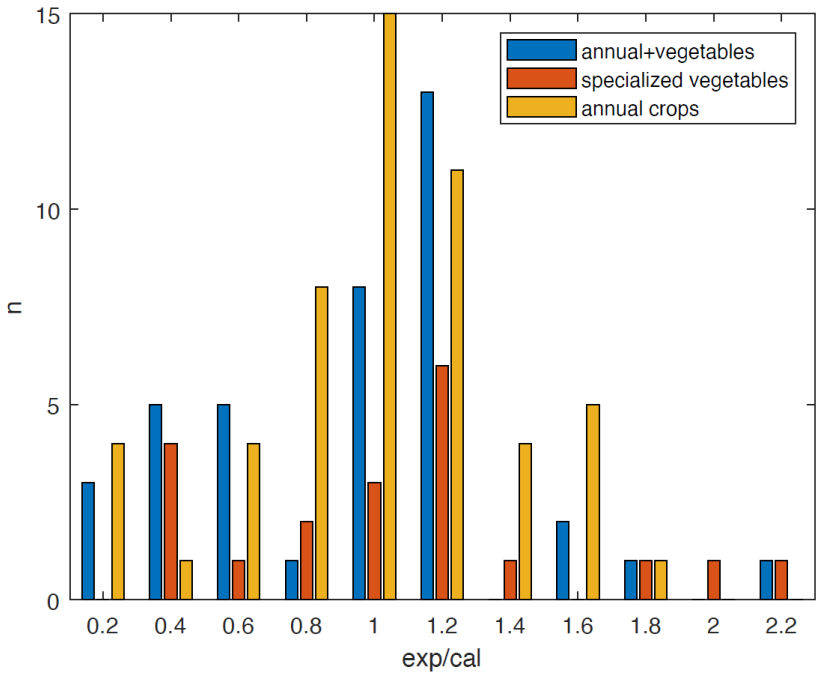

524

525 Figure 6: Distribution of ratios between expected and calculated surfaces in Miribel catchment.

526 For grassland landscapes, expected/calculated ratios were also centered on the mean
527 value 1 (fig. 7), giving quite realistic landscapes regarding farms needs. Moreover, a few
528 differences were visible, noticeably in the area of first priority for productive animal pastures,
529 where fields were not subdivided like farmers can do to adjust seasonal livestock needs to
530 vegetation production. Deviations from true landscapes mainly resulted from uniform patterns

of decision rules, not always adapted to account for local/seasonnal adaptations to farm plot configurations. In some instances, this reflected our choices for the implementations of the landscape models, mainly driven by the need to provide a sufficiently exhaustive but also simplified representation of agricultural landscapes allowing us to infer accessible input data.

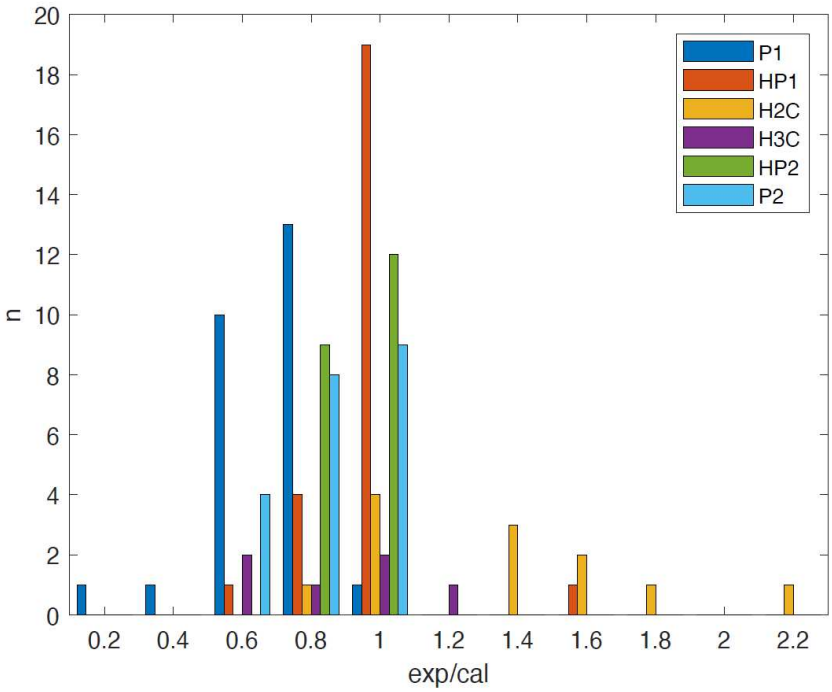

Figure 7: Distribution of ratios between expected and calculated surfaces in Autrans catchment. P1 : first priority pasture ; H : hay one cut ; H2C : hay two cuts ; H3 : hay three cuts ; P2 : second priority pasture.

4.4.2. WMWL modeling

The following figures confront calculated and observed data. For Miribel (fig. 8), the Nash-Sutcliffe efficiency (NSE) coefficient was 0.81. Model biases were not detected, as observed-calculated couples were regularly placed around the bisector line. For Autrans, similar patterns

were observed, although NSE was lower (NSE=0.56, fig. 9), yet above the 0.5 threshold agreed upon for model accuracy (Moriasi et al., 2007). Calculated water flows for Aiguebelette also fitted rather well with observed data (NSE=0.72, fig. 10). The main difference between the three catchments came from their sensitivity to loose deep water (as expected, the c_1 value corresponded to high impermeable territory at Autrans, tab. 2). We also noted a higher drainage dynamics at Miribel (high groundwater table delay λ value), according to the high drainage density in this annual cropland zone.

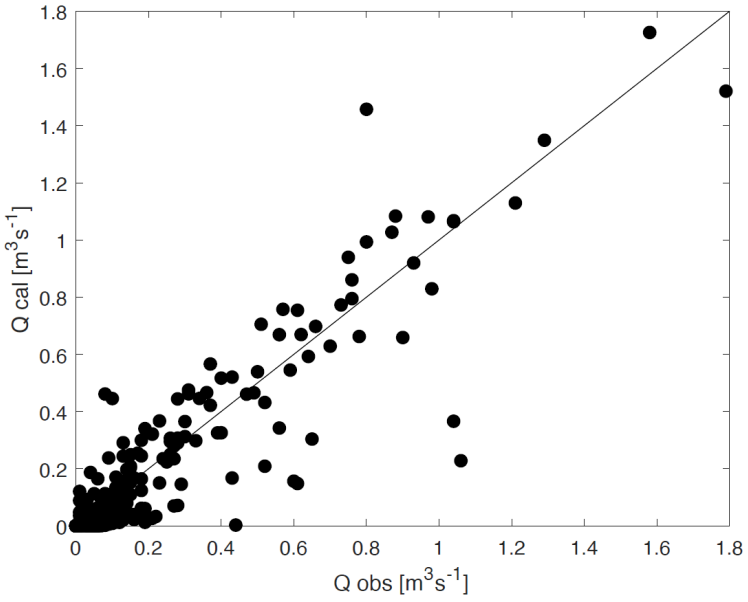

Figure 8: Observed and calculated water flow outputs in Miribel catchment.

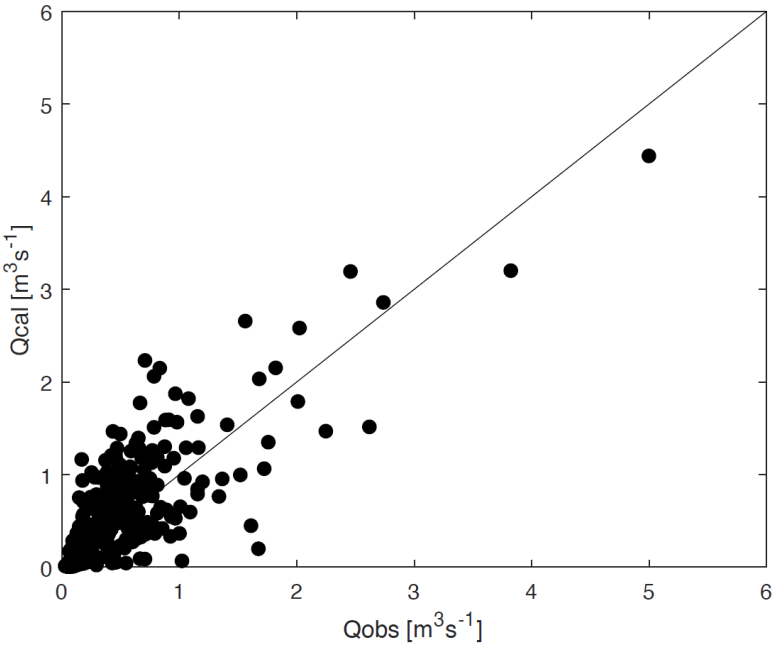

553

554 Figure 9: Observed and calculated water flow outputs in Autrans catchment.

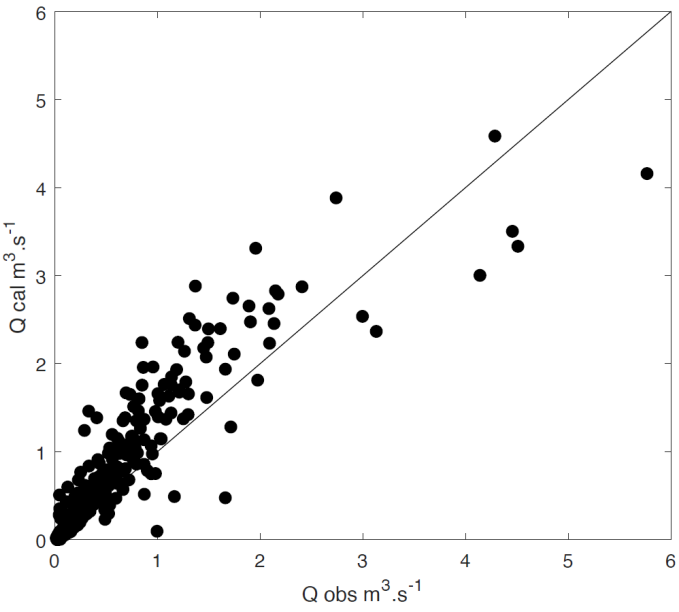

555

556 Figure 10: Observed and calculated water flow outputs in Aiguebelette catchment.

557

558 Global responses were also specific to the geographical contexts, and fitted well with the

559 hydrological patterns of the areas. Thus, hortonian runoff represented 12.5% of total outflows in
560 Miribel, and around 1% in the other two catchments. It was quite the same with saturation runoff
561 (9.6 % in Autrans, negligible elsewhere). In Autrans, peak flows came first from water table
562 drainage (89%) and secondly from urban runoff from impermeable surfaces (9%). In Aiguebelette,
563 rural overland flows were reduced ($< 1\%$). Considering the low number of WWML model
564 parameters, the various soils and agricultural conditions in which it was applied, the diversity of
565 hydrological processes taken into account, the efficiency of acceptable flow representations, as
566 well as the good agreements with the characteristics of the hydrosystems, we considered that
567 the underlying hypotheses about water balance and movement were founded.
568
569 **4.4.3. SSMT modeling**
570 Figure 11 gives an example of SSMT outputs. These are maps of Miribel catchment
571 showing the transfer of particles at different time steps τ following a winter DMEI, when the
572 plant cover was reduced and soil surfaces subject to crust waterproofing. Produced surface SM
573 decreased rapidly in one/two days.
574

575
576 Figure 11: Spatial particle distribution following a winter DMEI
577

4.4.3.1. Sub-surface transfer functions

For Miribel catchment, *SSTF*s were calculated for hortonian runoff for noteworthy DMEIs at $t_i = t - \tau_f$ producing high flow peaks during the crop season (fig. 12).

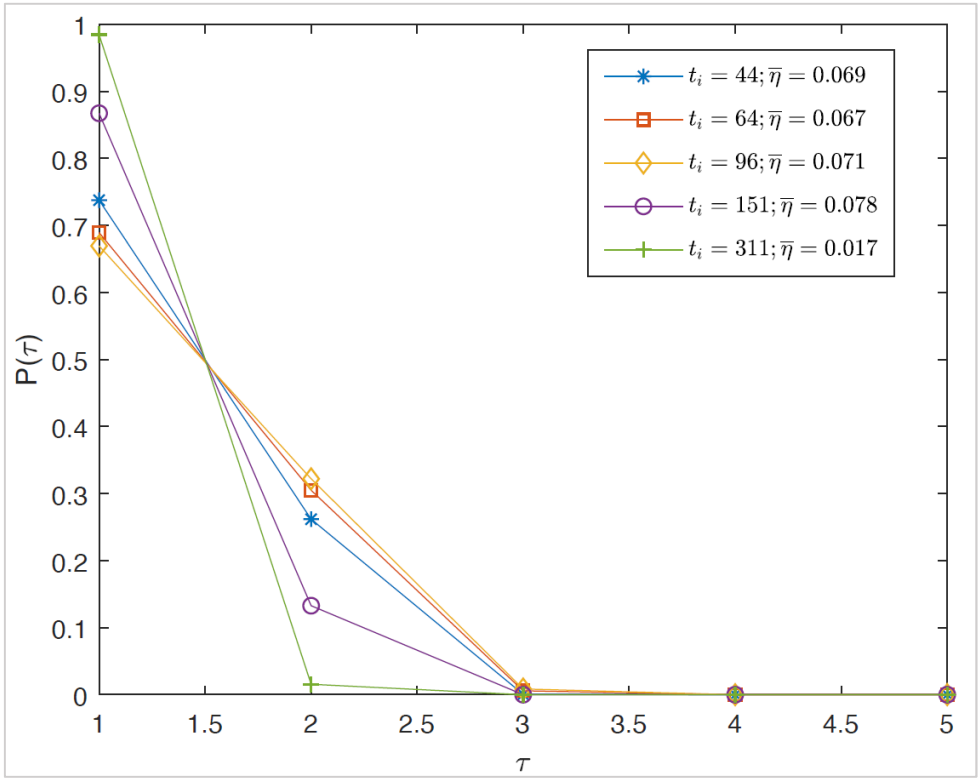

Figure 12: Transfer functions of hortonian surface runoff for several DMEIs and corresponding delivery ratios η.

During spring and early summer $t_i = 44, \ldots, 151$, *SSTF*s were rather similar, with delivery ratios $\eta(t_i)$ around 0.075. Considering the similarity of the spring *SSTF* responses, we considered that the *SSTF*($t_i = 44$) was a good representative of the spring transfer dynamics and used it for the whole spring season to predict Miribel SM flows from hortonian runoff. Following Boiffin et al (1988), hortonian runoff was modeled considering the extension of low-permeability

surface crusts (structures named F2) and the rearrangement of high-permeability soil surfaces (structures named F3), cf Appendix A, §7.5. In summer, no particle was generated because the soil surface permeability remained high (the mean extension area of F3 exceeded that of F2). The lowering of the water table and drying out of the drainage network led to a strong decrease of water flows (in wet conditions, the river length was nearly 40 Km; in summer, based on eq. 23, it was 500 m), so that the turbidity probe at the catchment outlet was not permanently covered by water flows. In early fall ($t_i = 311$), the drying out of the drainage network persisted but was lower than in summer (the drainage network length was around 10 % of its initial length). Due to the disconnection of active overland flow areas, the *SSTF* sharply decreased with reduced $\eta(t_i)$ (=0.02).

For Autrans catchment, several DMEIs were evaluated (fig. 13). Two main *SSTF* response patterns were described, with a first type in which distributions showed sharp decreases when $P(\tau_1) > 0.5$, and a second type with lower decrease. They corresponded to rapid losses when active areas were close to the river network, or differed transfer rates from more distant sources, respectively. The first sharp type was generated when the H_{vsa} variable source area (VSA) flows was greater than 1.5 $m^3.s^{-1}$. The delivery ratios also differed throughout the season according to hydrological conditions, with a general trend given by the statistical relationship $\eta(t_i) = 0.099H_{vsa}(t_i) + 0.051$ ($r^2 = 0.6^{**}$). Consequently, two *SSTF* types and the relationships between the delivery ratio and the variable source flow were introduced in $q_L(t)$, the lumped evaluation of EC flows.

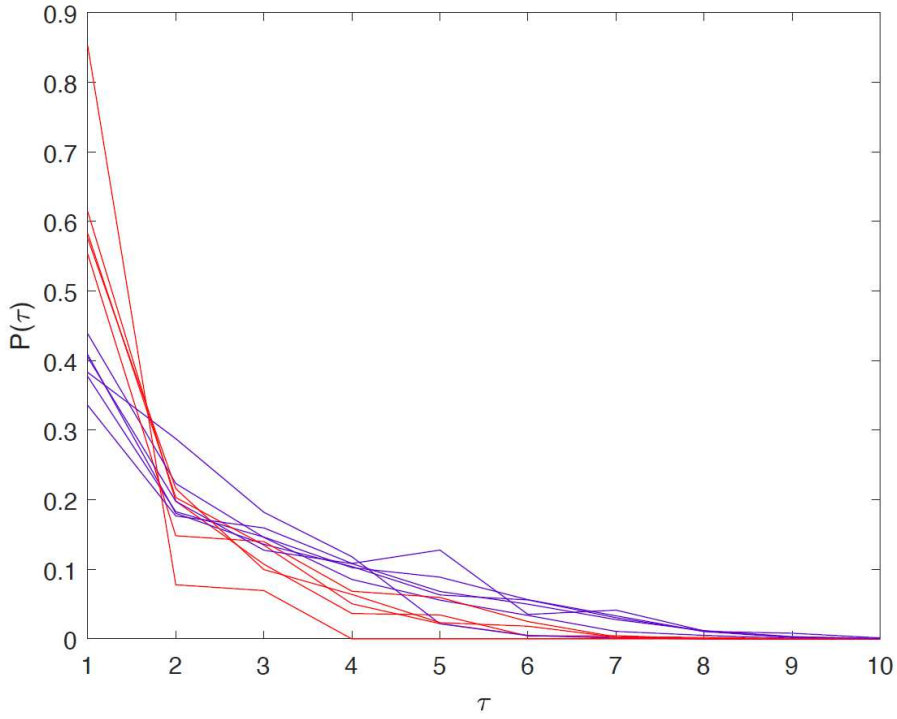

Figure 13: Transfer functions for saturation excess runoff in Autrans catchment. Red lines: type 1; green lines: type 2.

For the Aiguebelette catchment, *SSTF*s studied for different seasons ($t_i = 31, 64, 113, 167, 212$,315) were rather equivalent, with a sharp decrease similar to the one described in Miribel at $t_i = 311$ (fig.12), due to the fact that the water movements were essentially vertical and limited volumes moved laterally in this filtering context.

4.4.3.2. Modeling of matter outflows

At Miribel, turbidity probes operated until late spring, and data were collected to evaluate SSMT outputs (figure 14, NSE=0.73). One event (obs=2.51 ntu.d^{-1}; cal=1.40 ntu.d^{-1}) situated at the end of the modeled sequence reduced the NSE ratio. It corresponded to stochastic

622 conjunctions of the plowing, sowing or hoeing dates that probably led to lower F2-F3 differences.

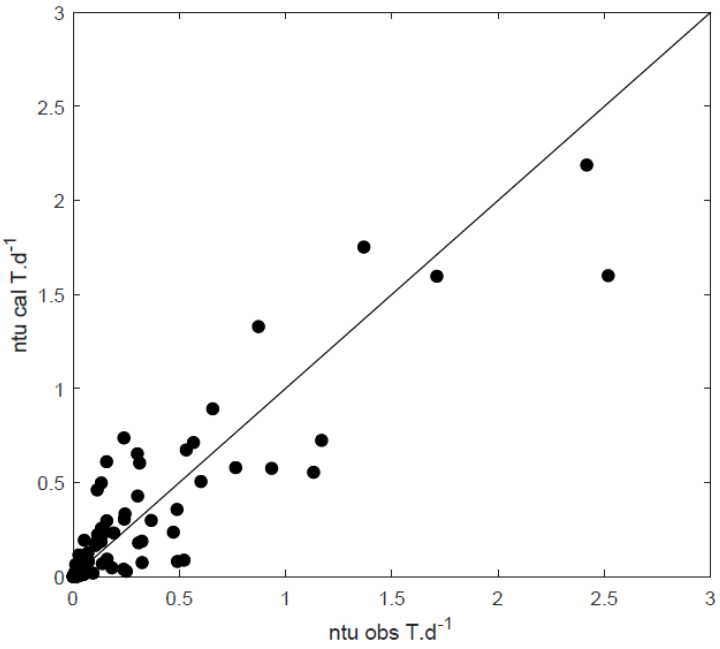

623

624

625 Figure 14: Observed and calculated SM flow outputs in Miribel catchment.

626

627 At Autrans, observed values were filtered according to the proportions of bacteroidales
628 markers of human and bovine origins (the bovine origin was dominant, ranging from 0.7 to 0.9%).
629 Observed and calculated EC values were confronted in fig. 15 (NSE=0.61). Even though
630 acceptable, efficiency was moderate, as often when comparing manual samples to daily
631 computations; the spatial variability of fecal populations can be large in river systems, with diurnal
632 variation (often by several orders of magnitude), as noted by EPA, 2010.

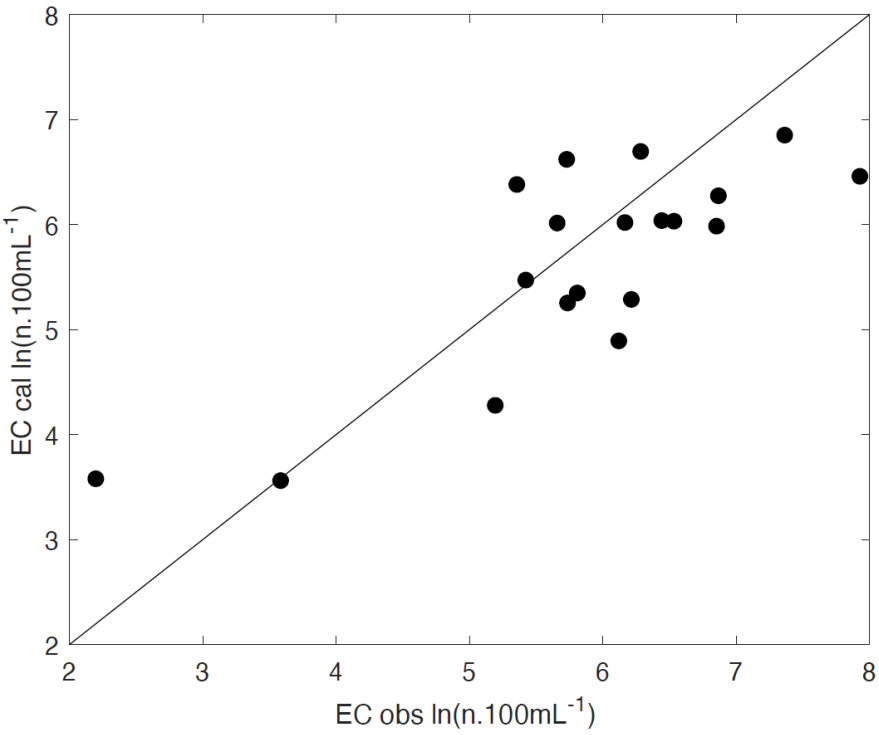

633

634 Figure 15: Observed and calculated EC flow outputs of Autrans catchment.

635

636 The solute transport in Aiguebelette was analyzed considering eq. 7 and 8 and the *GTF*
637 transfer distribution $P(\tau)$ associated to the λ parameter describing water table seepage. For
638 SM and particulate matter, we developed the lumped modeling schemes described in previous
639 studies for similar bank erosion situations (Trévisan et al. ,2019), considering that the production
640 function $m(t)$ was obtained from stores $s(t)$ related to the active river length and livestock
641 pressure, and wash-off $w(t)$ was associated with drainage flow and urban runoff. Fig. 16 gives
642 results obtained at Aiguebelette for solutes or suspended compounds recorded at the outlet.
643 NSEs were equal to 0.91, 0.92 and 0.90 for nitrogen, total phosphorus and SM, respectively.
644 Efficiencies were high, and residuals were regularly dispersed around bisectors.

Despite the variety of transferred compounds and modes of matter displacement, outflows were quite well reproduced by SSMT modeling, and provided evidence of the efficiency of OPALE outputs ($\eta(t_i)$, $s(t)$, $w(t)$, *SSFT* and *GTF*) in assessing the links between practices and water-related functions in agricultural landscapes.

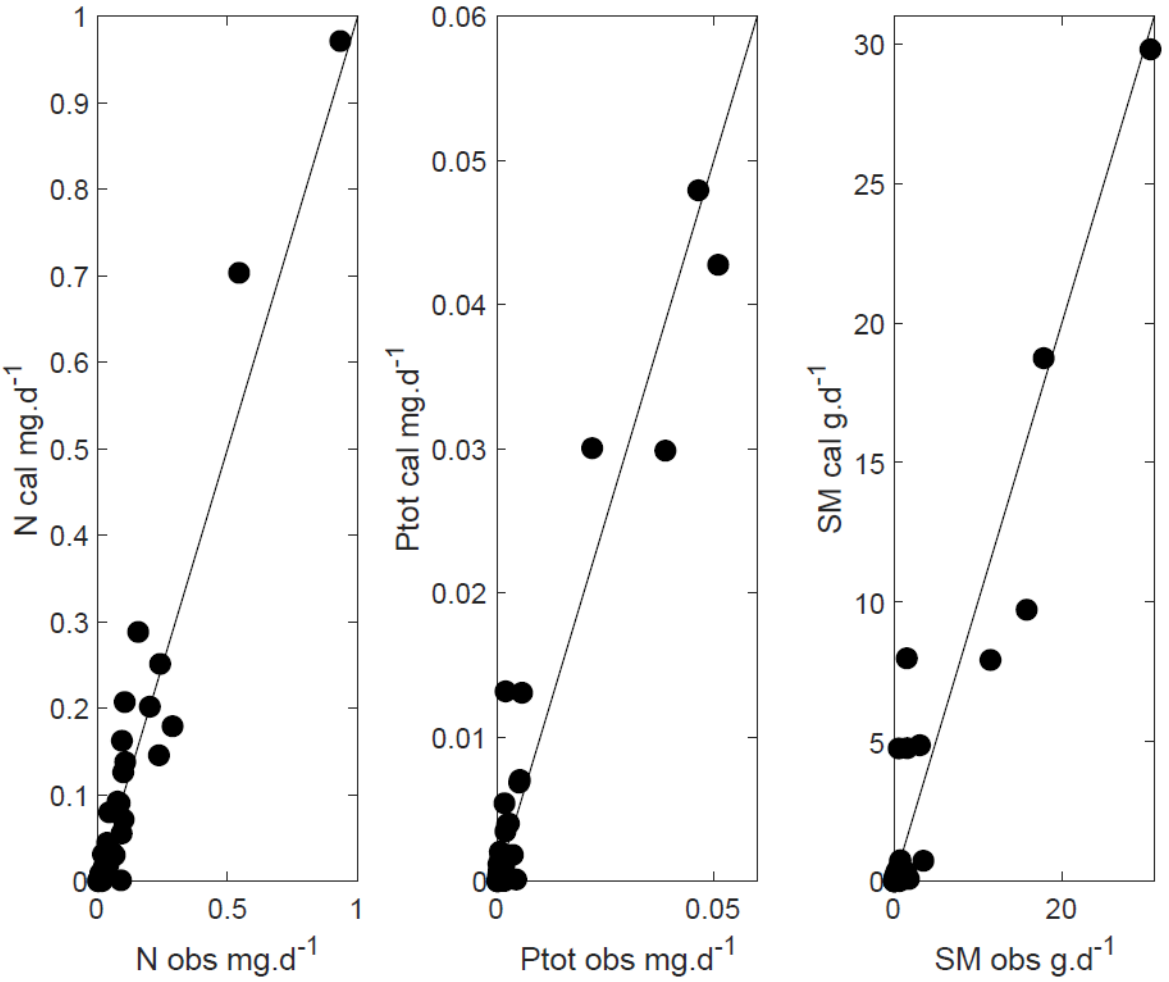

Figure 16: Observed and calculated N, P and SM flows of Aiguebelette catchment.

4.4.4. Landscape reconfigurations

653 The values of efficiency coefficients E_f are given in table 3.

Miribel (1) SM k=6	R+100 % Hoeing	R+10% annual crops	R+0.2 ha GFS	R+0.4 ha GFS	R+3.4 ha GFS	R+3.8 ha GFS	R+22 ha GFS	R+42 ha GFS	R+96 ha GFS
	0.05	0.13	0.14	0.09	0.24	0.20	0.39	0.45	0.71

Autrans (1) *E. Coli* k=6	R+10 ha cereals	R+25 ha cereals	R+ Hedges 10km WE	R+ Hedges 10km NS	R+ Hedges 10km NS+10km WE	R+ Hedges 20km NS	R+ Hedges 20km NS+10km WE
	0.1	0.02	0.10	0.24	0.26	0.29	0.33

Aiguebelette (2) SRP k=1	R+1.2km open drain 5 march	R+1.2km open drain 23 april	R+1.2km open drain 16 June	R+1.2km open drain 11 november
	-0.02	-1.18	-1.29	-0.27

654

655 Table. 3. Efficiency coefficients for landscape reconfigurations in the Miribel, Autrans and
656 Aiguebelette catchments. (1), overland flows; (2), hypodermical flow; k, number of DMEIs; R,
657 reference landscape; GFS, grass filter strips; WE, west-east; NS, north-south.

658

659 For the Miribel catchment, hoeing of all row crops slightly reduced SM flows, insofar as the
660 benefits are expected to be limited to the few weeks following hoeing in this context of high soil
661 crusting sensitivity. Efficiency is greater when the numbers of farming systems with annual crops

662 increase (in such sytems soil surfaces are much more protected from erosivity because
663 intercropping reduces the length of the periods when soils are non covered by aerial biomass,
664 whereas unprotected, compacted and emissive harvesting sites can be prolonged in vegetable
665 production depending on the market demand). The efficiency of landscape reconfiguration by
666 GFS increased with the GFS area, and increased sharply when GFS implementations were located
667 on areas where SM particles converged, in accordance with the need for better recognition and
668 monitoring of critical source areas (Heathwaite et al, 2005).

669 In Autrans, the extension of plowed surfaces increased the landscape efficiency against *E.*
670 *Coli* loads. This was probably explained by the reduced pressure of manure spreads, as these are
671 buried by plowing and thereby not sources of bacterial emissions from overland runoff (Sistani et
672 al, 2009; Meals et Braun, 2006). However, efficiency was lower for R+25ha than for R+10ha of
673 spring cereals. This can be attributed to the fact that the closer proximmity of pastures to the
674 river network when cereal production was enlarged increased the pressure and transfer dynamics
675 of *E. coli*. It is also conceivable that the extension of the cereal production area went together
676 with an increased risk of hortonian runoff. High-stemmed hedges increase landscape efficiency,
677 especially when hedges are planted in a NS direction (the direction perpendicular to the main
678 slope and the water flow direction). This suggests that the effects of hedges are mainly
679 attributable to the interception of surface runoff trajectories, firstly by increasing the re-
680 infiltration of runoff due to the greater evapotranspiration potential of hedges compared to
681 grasslands (Granier, 2007; Merot et al, 1999), and secondly by a trapping effect, which is debated
682 for bacteria (Vansteelant, 2004). These examples show how several landscape ecofunctionnalities

683 can be associated in order to rationally fight against water contamination, the proliferation of
684 grassland vole overgrowths, as well as better conditions for pasture, thanks to shading effects
685 associated with hedge networks.

686 Drainage of humid areas in Aiguebelette is concomitant with decreasing efficiency of
687 landscapes against the control of SRP flows from hypodermical transfers. The decrease is much
688 sharper during the growing season (April and June), when plant root systems are fully active,
689 compared to winter or autumn when evapotranspiration and nutrient uptake are low (Granier,
690 2007) and efficiency less deprecated.

691 # 5. Conclusion

692 Landscape eco-functionalities are related to agricultural uses and schedules (Wezel et al.,
693 2009 ; Gascuel-Odoux and Magda, 2015), and stakeholders use operational tools to assess the
694 incidence of global change (climatic perturbations, urbanization) and evaluate the adaptations of
695 farming systems or new land-use practices. A number of ecological infrastructures can be
696 implemented to control and protect water resources, such as filter strips (Dorioz et al., 2006),
697 interstitial hedgerows (Merot et al., 1999), riparian hedgerows (Zaimes et al., 2008), and
698 ecological infrastructures including meanders, marshes, etc. (Wang et al., 2004 ; Trévisan et
699 Periáñez, 2016). In practice, the efficiency of mitigation practices or landscape infrastructures
700 strongly depends on their position in the landscape, as well on cumulative effects (Wang et al.,
701 2004). OPALE – the tool presented in this article – was developed as an assessment tool of
702 landscape organization to meet such demands by addressing several scientific and operational
703 issues.

Landscapes are built from production objectives of farming systems and related decision rules; as such, they are the seat of water displacements commonly analyzed through the common concept of transfer functions, representing the distribution over time of elementary water volumes exported at catchment outlets (Haggerty et al., 2000 ; Hingray et al., 2009). This representation is well developed in catchment hydrology to predict water flows and associated signals (natural or artificial tracers) at the outlet of catchments, e.g., Nilo de Oliveira Nascimento et al. (1999), but also in river hydrology to evaluate channel organization and responses (Gooseff et al., 2003 ; Trévisan and Periáñez(2016). Despite available knowledge on the relationship between topographic patterns of catchments and the variability of their residence times (McGuire et al., 2005), eco-hydrology developments are expected to evaluate the relationships between landscape composition-structure and transfer patterns (McGuire and McDonnell, 2006). Our work is a contribution to such issues. It proposes several libraries aimed at *(i)* analyzing the dynamics of the restitution of water and associated matter to the catchment outlet from the explicit resolution of distributed water balances and particle tracking methods, and *(ii)* evaluating the efficiency of developed methods by using lumped modeling techniques and confronting them to a variety of real-world observations.

Operational issues mainly concern *(i)* the need for generic models adapted to a large geographical diversity of production systems, biophysical environments and landscape features, *(ii)* data accessibility, *(iii)* robustness of algorithms to avoid over-parameterization and over-fitting problems, and *(iv)* workable interfaces limiting I/O data manipulation as much as possible and allowing fast workflows from data configuration to diagnosis.

OPALE allowed for efficient evaluations of water and matter outflows and led to transfer functions and delivery ratios usable as synthetic indicators of the assessment of landscape functioning and eco-functionality.We demonstrated the effectiveness of OPALE procedures regarding such criteria through three diverse true-life cases in terms of agriculture, soil and hydrology conditions.

6. Aknowledgments

This research was funded by the TIPTOP-PSDR4 program, with the contribution of INRA, Région Auvergne-Rhône Alpes, IRSTEA and the FEADER and PEI-AGRI European Union funds.

7. Appendix A: WMWL model formulations

Hydraulic properties (field moisture capacity, saturated hydraulic conductivity) were computed using pedotransfer functions (Bruand et al., 2002).

7.1. Plant development model

The depth of the root zone was updated daily, applying the plant growth model developed by Gérard-Marchant et al. (2006) and in SMDR (2013). The first step of the computation was the evaluation of degree-day units DD:

$$DD = \begin{cases} T - T_b = \frac{T_{max} - T_b}{2} + \frac{T_{min} - T_b}{2} & \text{for} \quad T >= T_b \\ 0 \quad \text{for} \quad T < T_b, \end{cases} \tag{9}$$

where T, T_{max}, T_{min} are the mean daily, maximum and minimum temperatures [°C], respectively, and T_b a plant development threshold. Tables for T_b are given in the SMDR manual. Every day, the new computed DD value was added to the previous day value, following rules for stopping DD accumulation in case of negative temperatures or after harvest. Several formulas were applied to compute αD, a plant development factor (varying from 0 to 1 for maximum plant development), between different DD -accumulation thresholds (slow development DD_1; rapid development DD_2, maturity DD_3 and senescence DD_{max}):

$$G_1 = \frac{1}{DD_3}; \quad (10)$$

$$G_2 = \frac{1}{DD_3}\frac{DD_3 - DD_1}{DD_2 - DD_1}; \quad (11)$$

$$G_3 = -0.6\frac{1}{DD_{max} - DD_3} \quad (12)$$

The plant development factor was obtained from: $\alpha_D = G_1 DD$ if $DD < DD_1$ (slow development); $\alpha_D = 1 + G_2(DD - DD_2)$ if $DD_2 > DD > DD_1$ (rapid development); $\alpha_D = 1$ if $DD_3 > DD > DD_2$ (maturity); $\alpha_D = 1 + G_3(DD - DD_3)$ if $DD_{max} > DD > DD_3$ (senescence) and; $\alpha_D = 0$ if $DD > DD_{max}$ (dormancy).

Root depth ZR was then computed between ZR_{min} and ZR_{max}, the minimum and maximum values, from:

$$ZR = ZR_{min} + \alpha_D(ZR_{max} - ZR_{min}). \quad (13)$$

The ratio K_c between potential E_{tp} and real evapotranspiration E ($E = K_c E_{tp}$) was

764 calculated from minimum to maximum values following $K_c = K_{cmin} + \alpha D(K_{cmax} - K_{cmin})$. ZR
765 and K_c values are crop dependent and tabulated in SMDR (2013). A biomass indicator I_{bm} was
766 computed as follows:

767
$$\begin{cases} IBM(t) & = IBM(t-1) + \alpha_D * \beta & \text{if} DD(t) < DD_3 \\ & = 0 & \text{if} DD(t) > DD_3 \\ & = 0 & \text{if} t \geq \text{t(harvest)} \end{cases} \quad (14)$$

768 where β –varying from 0 to 1 and depending on soil moisture (Arnold and Forhrer, 2005)–
769 reduces plant development in case of water stress. Water stress was considered as soon as the
770 vadose zone moisture θ_{rz} dropped below θ_{eu}, the easily usable water reserve ($\theta_{eu} =$
771 $0.25(\theta_{cc} - \theta_{wp}) + \theta_{wp}$, where θ_{cc} and θ_{wp} are the field capacity and the wilting point,
772 respectively). The water stress predictor was obtained from $\beta = exp(5(\theta_{rz}/\theta_{eu} - 1))$.
773

774 ## 7.2. Drainage D

775 Excess water available for vertical or lateral movements W_e was obtained from $W_e =$
776 $max(0, W_{vz} - W_{cc})$, with W_{vz} the soil moisture and W_{cc} the moisture at field capacity [m].
777 Drainage D was obtained from (Arnold and Fohrer, 2005) by $D = W_e(1 - e^{-\frac{1}{\omega}})$, where the time
778 delay coefficient ω is deduced from $\omega = \frac{W_{sat} - W_{cc}}{K_{bot}}$, with W_{sat} the moisture at saturation [m],
779 K_{bot} the saturated hydraulic conductivity [m.day $^{-1}$] at the bottom of the vadose zone, given
780 by:

781
$$K_{bot} = k_m K_{sat}, \quad (15)$$

782 where k_m is a coefficient that accounts for the reduction of the vadose zone hydraulic

783 conductivity K_{sat}. At the end of each day iteration, the daily groundwater production $D(t)$ was
784 added to V_D, the deep water store: $V_D(t) = V_D(t-1) + D(t)$.
785
786 ## 7.3. Lateral flow L
787 Lateral flow $L(t)$ was given by $L(t) = \frac{2W_e K_{sat}}{(\theta_{sat} - \theta_{cc})d}$, where θ_{sat}, θ_{cc} are the soil
788 moisture at saturation [m.m $^{-1}$], and d the distance between two adjacent cells, respectively.
789 d was equal to l, the cell size of the computational square mesh in case of orthonormal flow
790 directions, and to $\sqrt{2}l$ when flow directions were north east, south east, south west or north
791 west. Lateral flows were routed to down-slope cells occupied by a river segment, following the
792 $D\infty$ algorithm (Tarboton, 1997) and cascade schemes (Kiesel et al., 2013).
793
794 ## 7.4. Variable source area surface flows
795 Following Obled and Zin (2004), effective rainfall was added daily to the vadose zone.
796 When the resulting moisture W_{vz} exceeded $W_{vz_{sat}}$ (the saturated soil moisture), the overland
797 flow H_{vsa} was computed by $H_{vsa} = W_{vz} - W_{vz_{sat}}$. At the end of each day iteration, the daily
798 production $H_{vsa}(t)$ was added to V_{vsa}, the VSA surface store: $V_{vsa}(t) = V_{vsa}(t-1) +$
799 $H_{vsa}(t)$.
800
801 ## 7.5. Hortonian surface flows
802 We considered that hortonian runoff mainly came from the crusted, low-permeability
803 area (Cerdan et al., 2002). The flow q infiltrated into crusted soils was obtained from (Jetten et

al., 1998):

$$q = \frac{K_c}{z_c}(\psi_u + h_0 + z_c), \quad (16)$$

where K_c is crust conductivity, z_c crust thickness, h_0 surface runoff depth and ψ_u root zone suction. ψ_u depends on soil moisture and was modeled by the Van Genuchten's equation:

$$\psi_u = \frac{[(\frac{\theta-\theta_{res}}{\theta_{sat}-\theta_{res}})^{\frac{-1}{m}}-1]^{\frac{1}{n}}}{\alpha} \quad (17)$$

where θ, θ_{res}, θ_{sat} are the vadose zone soil moisture, the residual water content and the corresponding moisture at saturation, respectively. n and α were parameters depending on texture conditions, and $m = 1 - \frac{1}{n}$. With I rainfall intensity, r the proportion of crusted soil [$m^2.m^{-2}$] and R rainfall depth, if $q < I$, the overland hortonian runoff H_{hor} was given by:

$$H_{hor} = rR\frac{I-q}{I}. \quad (18)$$

The degradation of the soil structure owing to the impact of raindrops at the soil surface produces a typical deposit structure named $F2$. Particles are rearranged by splash and sedimentation at the soil surface, a very-low-permeability crust is formed, and surface roughness and water retention decrease (Boiffin et al., 1988). However, as the plant cover increases along the crop season, $F2$ structures are reshaped and progressively rearranged by alternating moistening/desiccation phases or by biological activity, making way for high-permeability $F3$ structures. In addition, rainfall is redirected by leaves and stems to the collars of plants, where soil surface permeability is elevated. We therefore considered that soil crusting and plant development had opposite effects and we calculated the extension of crust deposits r (the

proportion of cell surface covered by crust deposits) with $r = max(0, F2 - F3)$.

We considered the extension of crust $F2$ by calculating:

$$F2 = \frac{R_{cum}}{c_{F2}+R_{cum}}, \quad (19)$$

where R_{cum} is cumulative rainfall, daily updated from the seeding date of annual crops, and c_{F2} an agricultural parameter. c_{F2} values were calculated from experimental surveys of crusting dynamics (Vansteelant et al., 1997 ; Lepilleur, 2017), given in supplementary material S4. F3 (varying from 0 to 1) was obtained from $F3 = \frac{I_{bm}}{I_{bm_M}}$, where I_{bm_M} (eq.14) was the maximum value of the biomass indicator at the time of annual crop harvest. At the end of each day iteration, the daily production $H_{hor}(t)$ was added to V_{hor}, the hortonian surface store: $V_{hor}(t) = V_{hor}(t-1) + H_{hor}(t)$.

7.6. River outflow

$V_D(t)$ and $V_{vsa}(t)$ and $V_{hor}(t)$ stores are subject to losses or transfer delays described by first-order kinetics (Arnold and Fohrer,2005). Daily drainage losses $L_D(t)$ directed to the external aquifer not included in the catchment balance were given by $L_D(t) = V_D(t-1)(1 - e^{-c_1 \Delta t})$, leading to:

$$L_D(t) = V_D(t-1)(1 - e^{-c_1}). \quad (20)$$

Outputs from hortonian $V_{hor}(t)$ or saturation $V_{vsa}(t)$ overflows directed to river segments were obtained from :

$$\begin{aligned} V_{hor}(t) &= V_{hor}(t-1)(1 - e^{-c_2}) \\ and \quad V_{vsa}(t) &= V_{vsa}(t-1)(1 - e^{-c_3}), \end{aligned} \quad (21)$$

844 respectively. Transfer delays linked to the internal aquifer seeping into river segments were
845 modeled considering long restitution periods τ_s. Following Hingray et al.(2009), seepage V_D^{out}
846 was given by calculating:

847 $$V_D(t) = (V_D(t) - L_D(t)) * \tau_s^{-\lambda}. \quad (22)$$

848 Following Gurnell (1978), the number of river segments (cells connected to the outlet) m
849 was given by the rounded value:

850 $$m = N_R(\frac{API}{API_{max}})^b, \quad (23)$$

851 where N_R was the maximum number of river cells, b a shape parameter, API the previous
852 pluviometric index

853 $$API = \sum_0^{i=15} [R(t-i) - ETP(t-i)], \quad (24)$$

854 and API_{max} the maximum pluviometric index ($i = i_{max}$).

855 The river outflow Q [$m^3.s^{-1}$] transferred to the catchment outlet was obtained by
856 calculating:

857 $$Q(t) = \frac{l^2}{24\times3600}\left[\sum_{i=1}^{\xi} R_i(t) + \sum_{i=1}^{m}\left(V_{D_i}(t) + V_{vsa_i}(t) + V_{hor_i}(t)\right)\right], \quad (25)$$

858 where l was the dimension of a cell [m], ξ the number of impervious cells in urban
859 areas, and $R_i(t)$ rainfall.

860

861 # 8. Appendix B: SSMT model formulation

862 We will successively consider particle build-up, wash-off and sink-source effects, i.e.,
863 biophysical processes contributing to particle mobilization, extinction or withdrawal. To save

computational time, particle build-up is evaluated under the Matlab environment during the period preceding a DMEI. We did not consider lateral exchanges between cells, as this is commonly done in the field of environemental studies for the evaluation of agricultural pressures (Massa et al, 2008). In the contrary, during the transfer period following a DMEI, wash-off and sink-source effects were evaluated in the Gama environement, considering cascade effects between upslope and downslope cells.

8.1. Particle build-up

Build-up stocks $s_k(t)$ are generated on computational cells k by agricultural pressure and depend on crop requirements and practices. We defined several proxies as substitute variables for the different kinds of build-up stocks.

We evaluated nutrient build-up $s_k(t)$, considering the net stock of nutrients from a rough balance between fertilizer supply, mineralization, and assimilation, all of them documented by tables provided by technical institutes for crop production and protection (COMIFER, 2013). N leaching was evaluated from Burn's model (Burns, 1974). EC stocks were evaluated for grasslands, taking proportional links between fecal populations and N inputs from farm effluent spreading into account. EC inputs from deciduous and perennial forest wildlife were not excluded. Total nutrient needs, daily rates of net assimilation and EC particle patterns are given in supplementary material S2. We hypothesized that SM stocks $s_k^m(t)$ were produced by impermeable soil surface structures. They were evaluated by calculating $s_k^m(t) = max(0, F2_k(t) - F3_k(t))$, where $F2_k(t)$ and $F3_k(t)$ are the extents of continuous and discontinuous crusts, respectively (see

885 Appendix A). Depending on their nature, particle stocks are not equally available for all water
886 components. Except for surface flows where N, P, EC and SM can potentially be displaced from
887 upstream to downstream cells, particle displacement by subsurface flows was restricted to N and
888 soluble P, and only to N particles in the deepest water tables. The aim was to account for trapping
889 and filtering effects acting on EC and SM (Muirhead et al., 2006 ; Dorioz et al., 2006) and for lower
890 soluble P adsorption onto organic matter-enriched environments such as topsoils (Jarvie et al.,
891 2005). The stock distributions of the different hortonian runoff $h_k^{hor}(t)$, VSA runoff $h_k^{vsa}(t)$,
892 subsurface $l_k(t)$ and drainage $d_k(t)$ flows were calculated considering their respective
893 proportions. For example:

894 $$s_k^{hor}(t) = s_k(t)\frac{h_k^{hor}(t)}{h_k^{hor}(t)+h_k^{vsa}(t)+l_k(t)+d_k(t)} \quad (26)$$

895 gave the amount of particles available for hortonian runoff $s_k^{hor}(t)$.

896

897 ## 8.2. Particle wash-off

898 During the transfer period $\tau = (0, \dots, \tau_f)$ and referring to salt redistribution (Burns,
899 1974) or soil-water relationships (Holzbecher, 2012), we considered a generalized formulation of
900 the $w_k(t-\tau)$ wash-off:

901 $$w_k(t-\tau) = \left(\frac{h_k(t-\tau)}{h_k(t-\tau)+\delta}\right)^r, \quad (27)$$

902 where δ was a mobility coefficient for particulate or solute matters, $h_k(t-\tau)$ a water flow
903 component, r the half of soil depth in case of solutes (equals to one otherwise).

904

8.3. Sinks-sources

The store of particles was updated throughout the transfer period. Sink effects were considered:

$$s_k(t-\tau) = s_k(t-\tau-1) - a_k(\tau) - d_k(\tau) - k_d(\tau), \quad (28)$$

where, if suited to particle nature, $a_k(\tau)$ was the net assimilation rate (the balance between daily mineralization and daily assimilation), $d_k(\tau)$ denitrification and $k_d(\tau)$ mortality.

The production function $m_k(t-\tau)$ of particles available to down-slope transfer was obtained by calculating:

$$m_k(t-\tau) = s_k(t-\tau)w_k(t-\tau) - r_k(\tau) + e_k(\tau), \quad (29)$$

giving the amount of particles originating from cell k and transferred during τ steps to down-slope cells $k+1$, where if suited to particle nature, $r_k(\tau)$ was retention and $e_k(\tau)$ an additional wash-off source.

Daily assimilation rates $a_k(\tau)$ of N and P were estimated considering the length of plant development phases. De-nitrification losses $d_k(\tau)$ were accounted for when soil moisture exceeded the field-capacity threshold (Nicolardot et al, 1996). Following COMIFER (2013), they were evaluated by calculating $d_k(\tau) = c_d s_k^N(t-\tau)$ where c_d is a de-nitrification constant and $s_k^N(t-\tau)$ the initial N store, respectively. EC decay $k_d(\tau)$ was accounted for during the growth and maturity phases of plant development from experimental counts of EC populations on meadow canopies following manure application (Trevisan et al., 2002). Particles from SM production $m_k^{SM}(t-\tau)$ were retained when overland flows crossed filtering infrastructures. Based on experimental data obtained by (Trévisan and Dorioz, 2001), we applied a first-order

926 kinetic to calculate the value of the retention function: $r_k(\tau) = m_k^{SM}(t-\tau)e^{-\beta L}$, where L is
927 the width of the crossed infrastructure and β a length parameter. Additional SM particles can
928 come from runoff concentrations (Cerdan et al., 2002). As linear relationships often occur
929 between erosion rates and runoff amounts (Mamedov et al. , 2016 ; Pardini et al, 2016), we
930 considered the source effects with additional production $e_k(\tau) = \theta\hat{h}_k(t-\tau)$, where θ is a
931 proportionality factor and $\hat{h}_k(t-\tau)$ the surface runoff volume accumulated up-slope of cell k.
932

933 # 9. Appendix C: SSMT validation

934 To simplify formulations, we considered outflows provided by a transfer period of
935 duration $\tau_f = 1$. Based on eq. 3, 4 and 7, we calculated:

936
$$\begin{cases} q_L(t) & = \eta(t-\tau_f)\sum_1^k m_k(t) * P(1) \\ & = \frac{\sum_1^{\tau_1} q(\tau_1)}{\sum_1^k s_k(t-\tau_f)w_k(t-\tau_f)}\sum_1^k m_k(t-\tau_f)P(1) \\ & = \frac{\sum_1^{\tau_1} q(\tau_1)}{\sum_1^k s_k(t-\tau_f)w_k(t-\tau_f)}\sum_1^k s_k(t-\tau_f)w_k(t-\tau_f)P(1) \\ & = \sum_1^{\tau_1} q(\tau_1)\frac{q(\tau_1)}{\sum_1^{\tau_1} q(\tau_1)} \\ & = q(\tau_1). \end{cases} \quad (30)$$

937 We retained that the lumped modeling of particle outflows equaled the SSMT particle count.
938

939 # 10. References

940 AFNOR, 1990. Eaux, méhodes d'essais. Technical Report. ISBN 2121790411.

941 Arnold, J., Fohrer, N., 2005. Swat2000 : Current capabilities and research opportunities in applied
942 watershed modelling. Hydrological Processes 19, 563–572.

943 Benoît, M., Rizzo, D., Marraccini, E., Moonen, A., Galli, M., Lardon, S., Rapey, H., Thenail, C., Bonari, E.,
944 2012. Landscape agronomy: a new field for addressing agricultural landscape dynamics. Landscape Ecology
945 27, 1385–1394.

946 Boiffin, J., Papy, F., Eimberck, M., 1988. Influence des systèmes de culture sur les risques d'érosion par
947 ruissellement concentré. I. – Analyse des conditions de déclenchement de l'érosion. Agronomie 8, 663–
948 673.

949 Bruand, A., Perez Fernandez, P., Duval, O., Quétin, P., Nicoullaud, B., Gaillard, Raison, L., Pessaud, J.,
950 Prud'Homme, L., 2002. Estimation des propriétés de rétention en eau des sols : utilisation de classes de
951 pédotransfert après stratifications texturale et texturo-structurale. Etude et Gestion des Sols 9, 105–126.

952 Burns, I., 1974. A model for predicting the redistribution of salts applied to fallow soils after excess rainfall
953 orevaporation. Journal of Soil Science 25, 165–177.

954 Cerdan, O., Le Bissonnais, Y., Couturier, A., Saby, N., 2002. Modelling interrill erosion in small cultivated
955 catchments. Hydrol. Process. 16, 3215–3226.

956 Chaplin-Kramer, R., Hamel, P., Sharp, R., Kowal, V., Wolny, S., Sim, S., Mueller, C., 2016. Landscape
957 configuration is the primary driver of impacts on water quality associated with agricultural expansion.
958 Environmental Research Letters 11.

959 Chenouard, N., Smal, I., de Chaumont, F., et al., 2014. Objective comparison of particle tracking methods.
960 Nat Methods 11, 281–289.

961 COMIFER, 2013. Calcul de la fertilisation azotée. Guide méthodologique pour l'établissement des
962 prescriptions locales. Cultures annuelles et prairies. Comifer, ISBN 978-2-910393-09-0.

963 Dorioz, J., Pilleboue, E., Ferhi, A., 1989. Dynamique du phosphore dans les bassins versants: importance
964 des phénomènes de rétention dans les sédiments. Water Research 2, 147–158.

965 Dorioz, J.M., Wang, D., Poulenard, J., Trévisan, D., 2006. The effect of grass buffer strips on phosphorus
966 dynamics. A critical review and synthesis as a basis for application in agricultural landscapes in France.
967 Agriculture, Ecosystems & Environment 117, 4–21.

968 Dunne, T., Moore, T., Taylor, C., 1975. Recognition and prediction of runoff-producing zones in humid
969 regions. Hydrological Sciences Bulletin. 20, 305–327.

970 Dury, J., Schaller, N., Garcia, F., Reynaud, A., Bergez, J., 2012. Models to support cropping plan and crop
971 rotation decisions. A review. Agronomy for sustainable development 32 (2), 567–580.

972 Edmonds, J., Karp, R.M., 1972. Theoretical improvements in algorithmic efficiency for network flow
973 problems. Journal of the ACM (JACM) 19, 248–264.

974 EPA, 2010. Sampling and consideration of variability (temporal and spatial) for monitoring of recreational
975 water, EPA-823-R-10-005. Technical Report. U.S. Environmental Protection Agency. Office of Water.

976 Evrard, O., Cerdan, O., Van Wesemael, B., Chauvet, M., Le Bissonnais, Y., et al., 2009. Reliability of an
977 expert-based runoff and erosion model: Application of STREAM to different environments. CATENA 78,
978 129–141.

979 Gascuel-Odoux, C., Magda, D., 2015. Gérer les paysages et les territoires pour la transition agroécologique.
980 Innovations Agronomiques 43, 95–106.

981 Gérard-Marchant, P., Hively, W.D., Steenhuis, T.S., 2006. Distributed hydrological modelling of total
982 dissolved phosphorus transport in an agri-cultural landscape, part I: distributed runoff generation.
983 Hydrology and Earth System Sciences Discussions, European Geosciences Union, 10, 245–261.

984 Gooseff, M.N., Wondzell, S.M., Haggerty, R., Anderson, J., 2003. Comparing transient storage modeling
985 and residence time distribution (RTD) analysis in geomorphically varied reaches in the Lookout Creek basin,
986 Oregon, USA. Advances in Water Resources 26, 925–937.

Gurnell, A., 1978. The dynamics of a drainage network. Nordic Hydrology 9, 293 – 306.

Granier, A., 2007. Rôle des prairies dans le cycle de l'eau. Comparaison avec la forêt. Fourrages 192, 399–408.

Grillot, M., Guerrin, F., Gaudou, B., Masse, D., Vayssières, J., 2018. Multi-level analysis of nutrient cycling within agro-sylvo-pastoral landscapes in West Africa using an agent-based model. Environmental Modelling & Software, 107, 267-280.

Haggerty, R., McKenna, S.A., Meigs, L.C., 2000. On the late-time behavior of tracer test breakthrough curves. Water Resources Researh 36(12), 3467–3479.

Haggerty, R., Wondzell, S., Johnson, M., 2002. Power-law residence time distribution in the hyporheic zone of a 2nd-order mountain stream. Geophys. Res. Lett. 29, 18–1–18–4.

Halliez G, Renault F, Vannard E, Farny G, Lavorel S, Giraudoux P (2015) Historical agricultural changes and the expansion of a water vole population in an Alpine valley. Agriculture, Ecosystems and Environment 212 : 198-206.

Harbaugh, A.W., 2005. Modflow, the U.S. Geological survey modular ground-water model. The ground-water flow process. U.S. Geological Survey Techniques and Methods 6-A16 .

Hatt, S., Boeraeve, F., Artru, S., Dufrêne, M., Francis, F., 2018. Spatial diversification of agroecosystems to enhance biological control and other regulating services: an agroecological perspective. Science of the Total Environment 621, 600–611.

Heathwaite, A.L., Quinn, P.F., Hewett, C.J.M., 2005. Modelling and managing critical sources areas of diffuse pollution from agricultural land using flow connectivity simulation. Journal of Hydrology 304, 446-461.

1008 Hingray, B., Picouet, C., Musy, A., 2009. Hydrologie, 2. Une science pour l'ingénieur. Presses
1009 Polytechniques et Universitaires Romandes.

1010 Holzbecher, E., 2012. Environmental Modeling using MATLAB. ISBN 978-3-642-22042-5, Springer Ed.

1011 Houet, T., Schaller, N., Castets, M., Gaucherel, C., 2014. Improving the simulation of fine-resolution
1012 landscape changes by coupling top-down and bottom-up land use and cover changes rules. International
1013 Journal of Geographical Information Science 28, 1848–1876.

1014 Jarvie, H., Jurgens, M., Williams, R., Neal, C., Davies, J., Barrett, C., White, J., 2005. Role of river bed
1015 sediments as sources and sinks of phosphorus across two major eutrophic UK river basins: the Hampshire
1016 Avon and Herefordshire Wye. Journal of Hydrology 304, 51–74.

1017 Jetten, V.G., De Roo, A.P.J., Guerif, J., 1998. Sensitivity of the model LISEM to variables related to
1018 agriculture. Environmental Change, vol. 55, 339–350.

1019 Jiang, J., Liang, Q., Xia, X., 2019. A Physical-Based Particle-Tracking Scheme for Non-Point Source
1020 Particulate Pollutants Wash-off and Transport Processes in Urban Impervious Surfaces, in: AGU Fall
1021 Meeting Abstracts, pp. H13L–1874.

1022 Josselin, D., Janin, C., Bolot, J., 1999. Proposition d'une lecture territoriale des flux agricoles. Revue
1023 Géographique de l'Est. 39, 207–216.

1024 Kiesel, J., Schmalz, B., Brown, G., Fohrer, N., 2013. Application of a hydrological-hydraulic modelling
1025 cascade in lowlands for investigating water and sediment fluxes in catchment, channel and reach. J. Hydrol.
1026 Hydromech. 61, 334–346.

1027 Lafforgues, A., 1977. Inventaire et examen des processus élélmentaires de ruissellement et d'infiltration
1028 sur parcelles. Cah. ORSTOM, sér. Hydrol. XIV - 4.

1029 Langhammer, M., Thober, J., Lange, M., Frank, K., Grimm, V., 2019. Agricultural landscape generators for
1030 simulation models: a review of existing solutions and an outline of future directions. Ecological Modelling
1031 393, 135–151.

1032 Lellay, M., 2006. Modélisation hydrologique dans un contexte de variabilité hydro-climatique. Thèse.
1033 Institut National Paris Grignon.

1034 Lepilleur, H., 2017. L'imperméabilisation de la surface du sol. ESA Angers, 53p. Master's thesis.

1035 Mamedov, A., Warrington, D., Levy, G., 2016. Soil erosion-runoff relationships: insights from laboratory
1036 studies. Geophysical Research Abstracts 18.

1037 Marie, M., Bensaid, A., Delahaye, D., 2016. Le rôle de la distance dans l'organisation des pratiques et des
1038 paysages agricoles : l'exemple du fonctionnement des exploitations laitières dans l'arc atlantique.
1039 Cybergeo: European Journal of Geography. DOI : 10.4000/cybergeo.22366.

1040 Martel, G., Aviron, S., Joannon, A., Lalechère, E., Roche, B., Boussard, H., 2017. Impact of farming systems
1041 on agricultural landscapes and biodiversity: from plot to farm and landscape scales. European Journal of
1042 Agronomy . doi:https://doi.org/10.1016/j.eja.2017.07.014.

1043 Massa, F., Gascuel-Odoux, C., Mérot, P., Baudry, J., Beduneau, G., Blondel, R., Durand, P., Tico, S., Troccaz,
1044 O., 2008. Territ'eau, une méthode et des outils pour améliorer la gestion des paysages agricoles en vue de
1045 préserver la qualité de l'eau. Ingénieries EAT, Numéro spécial Azote, phosphore et pesticides, 115–132.

1046 Mauffret, A., Caprais, M., Gourmelon, M., 2012. Relevance of bacteroidales and f-specific RNA
1047 bacteriophages for efficient fecal contamination tracking at the level of a catchment in france. AEM 78,
1048 5143–5152.

1049 McGuire, K.J., McDonnell, J.J., 2006. A review and evaluation of catchment transit time modeling. Journal
1050 of Hydrology 330, 543–563.

1051 McGuire, K.J., McDonnell, J.J., Weiler, M., Kendall, C., McGlynn, B.L., Welker, J.M., Seibert, J., 2005. The
1052 role of topography on catchment-scale water residence time. Water Resources Research 41, W05002.
1053 doi:10. 1029/2004WR003657.

1054 Meals D.W., Braun D.C., 2006. Demonstration of methods to reduce E-coli runoff from dairy manure
1055 application sites. Journal of Environmental Quality 35, 1088-1100.

1056 Me, W., Hamilton, D.P., McBride, C.G., Abell, J.M., Hicks, B. J., 2018. Modelling hydrology and water quality
1057 in a mixed land use catchment and eutrophic lake : effect of nutrient load reductions and climate change.
1058 Environmental Modelling & Software, 109, 114-133.

1059 Merot, P., Gascuel-Odoux, C., Walter, C., Zhang, X., Molenat, J., 1999. Influence du réseau de haies des
1060 paysages bocagers sur le cheminement de l'eau de surface. Revue des sciences de l'eau 12(1), 23–44.

1061 Moriasi, D.N., Arnold, J.G., Van Liew, M.W., Bingner, R.L., Harmel, R.D., Veith, T.L., 2007. Model evaluation
1062 guidelines for systematic quantification of accuracy in watershed simulations. Transactions of the ASABE
1063 50, 885 – 900.

1064 Moussa, R., Voltz, M., Andrieux, P., 2002. Effects of the spatial organization of agricultural management
1065 on the hydrological behaviour of a farmed catchment during flood events. Hydrological Processes 16, 393–
1066 412.

1067 Muirhead, R., Collins, R., Bremer, P., 2006. Numbers and transported state of Escherichia coli in runoff
1068 direct from fresh cowpats under simulated rainfall. Letters in Applied Microbiology 42, 83–87.

1069 Nicolardot, B., Mary, B., Houot, S., Recous, S., 1996. La dynamique de l'azote dans les sols cultivés. in
1070 Maîtrise de l'azote dans les agrosystèmes, Annales colloques INRA 83. Reims (France), 19-20 nov, pp. 87–
1071 103.

1072 Obled, C., Zin, I., 2004. TOPMODEL : principes de fonctionnement et application. La Houille Blanche 1, 65–
1073 76.

1074 Nilo de Oliveira Nascimento, E., Yang, X., Makhlouf, Z., Michel, C., 1999. R3J: a daily watershed model with
1075 three free parameters. Hydrological Sciences Journal 44, 263–277.

1076 Pardini, G., Gispert, M., Emran, M., Doni, S., 2016. Rainfall/runoff/erosion relationships and soil properties
1077 survey in abandoned shallow soils of NE Spain. Journal of Soils and Sediments 17(2).

1078 Petitqueux, C., 2017. Organisation agropaysagère du Val du Méaudret : rôles des acteurs territoriaux et
1079 état des structures paysagères. ENSA Bordeaux, 93p. Master's thesis.

1080 Pezet, F., 2014. Bilans et transferts de phosphore dans le bassin versant du lac du Bourget : caractérisation,
1081 interprétation et modélisation des flux. Université de Savoie, 256p. Ph.D. thesis.

1082 Poggi, S., Vinatier, F., Hannachi, M., Sanz Sanz, E., Rudi, G., 2021. How can models foster the transition
1083 towards future agricultural landscapes? Advances in Ecological Research 10.1016/bs.aecr.2020.11.004.

1084 Poulenard, J., Perrette, Y., Fanget, B., Quétin, P., Trévisan, D., Dorioz, J., 2009. Infrared spectroscopy tracing
1085 of sediment sources in a smallrural watershed (French Alps). Science of the Total Environment 407, 2808–
1086 2819.

1087 Rizzo, D., Therond, O., Lardy, R., Murgue, C., Leenhardt, D., 2019. A rapid, spatially explicit approach to
1088 describe cropping systems dynamics at the regional scale. Agricultural Systems 173, 491–503.

1089 Sarrazin, B., 2012. MNT et observations multi-locales du réseau de drainage d'un petit bassin versant rural
1090 dans une perspective d'aide à la modélisation spatialisée. Ph.D. thesis. Grenoble.

1091 Schwanghart, W., Kuhn, N., J., 2010. TopoToolbox: a set of Matlab functions tor topographical analysis.
1092 Environmental Modelling & Software 25, 770–781.

1093 SMDR, 2013. SMDR The Soil Moisture Distribution and Routing Model. Cornell University, ITHACA. NY
1094 14853-USA.

1095 Sistani, K.R., Torbert, H.A., Way, T.R., Bolster, C.H., Pote, D.H., Warren, J.G., 2009. Broiler Litter Application
1096 Method and Runoff Timing Effects on Nutrient and Losses from Tall Fescue Pasture. Journal of
1097 Environmental Quality 38, 1216-1223.

1098 Taillandier, P., Gaudou, B., Grignard, A., Huynh, Q., Marilleau, N.P., Caillou, P., Philippon, D., Drogoul, A.,
1099 2019. Building, composing and experimenting complex spatial models with the gama platform.
1100 Geoinformatica 23, 299–322.

1101 Taillandier, P., Therond, O., Gaudou, B., 2012. A new BDI agent architecture based on the belief theory.
1102 Application to the modelling of cropping plan decision-making, in: International environmental modelling
1103 and software society (iEMSs).

1104 Takken, I., Beuselinck, L., Nachtergaele, J., Govers, G., Poesen, J., Degraer, G., 1999. Spatial evaluation of
1105 a physically based distributed erosion model (LISEM). Catena 37, 431–447.

1106 Tarboton, D., 1997. A new method for the determination of flow directions and contributing areas in grid
1107 digital elevation models. Water Resources Research 33, 309–319.

1108 Thenail, C., Joannon, A., Capitaine, M., Souchère, C., Mignolet, C., Schermann, N., Di Pietro, F., Pons, Y.,
1109 Gaucherel, C., Viaud, V., 2009. The contribution of crop-rotation organization in farms to crop-mosaic
1110 patterning at local landscape scales. Agriculture, Ecosystems & Environment 131, 207–219.

1111 Trévisan, D., Dorioz, J., 2001. Bandes herbeuses et lutte contre la pollution diffuse agricole. critère
1112 d'efficacité et conditions d'implantation. CIPEL Campagne 2000, 231–259.

1113 Trévisan, D., Giguet-Covex, G., Sabatier, P., Quétin, P., Arnaud, F., 2019. Coupling indicators and lumped-
1114 parameter modeling to assess suspended matter and soluble phosphorus losses. Science of the Total
1115 Environment 650, 3027–3040.

1116 Trévisan, D., Periáñez, R., 2016. Coupling catchment hydrology and transient storage to model the fate of

1117 solutes during low-flow conditions of an upland river. Journal of Hydrology 534, 317–325.

1118 Trévisan, D., Vansteelant, J., Dorioz, J., 2002. Survival and leaching of fecal bacteria after slurry spreading
1119 on mountain hay meadows: consequences for the management of water contamination risk. Water
1120 Research 36, 275–283.

1121 Vanier, M., 1995. The manufacturing process of territories in the Rhône-Alpes region actors, myths and
1122 practices. Géocarrefour 70-2, 93–103.

1123 Vansteelant, J., Trévisan, D., Perron, L., Dorioz, J., Roybin, D., 1997. Conditions d'apparition du
1124 ruissellement dans les cultures annuelles de la région lémanique. Relations avec le fonctionnement des
1125 exploitations agricoles. Agronomie 17, 65–82.

1126 Vansteelant, J.Y., 2004. Évaluation des risques de contaminations microbiologiques liés aux épandages de
1127 matières organiques sur prairies de montagne. Thèse de l'Université de Savoie, 194p.

1128 Wallach, D., Makowski, D., Jones, J., Brun, F., 2013. Working with Dynamic Crop Models: Methods, Tools
1129 and Examples for Agriculture andEnvironment. Academic Press.

1130 Wang, D., Dorioz, J.M., Trévisan, D., Braun, D.C., Windhausen, L.J., Vansteelant, J.Y., 2004. Using a
1131 landscape approach to interpret diffuse phosphorus pollution and assist with water quality management
1132 in the basins of lake Champlain (Vermont) and lake Léman (France). in Lake Champlain : partnership and
1133 research in the new millenium. Manley eds., Kluwer acad., 59 –189.

1134 Wezel, A., Bellon, S., Doré, T., Vallod, D., David, C., 2009. Agroecology as a science, a movement and a
1135 practice. A review. Agron. Sustain. Dev. DOI: 10.1051.

1136 World Reference Base for Soil Resources, 2014. International soil classification system for naming soils and
1137 creating legends for soil maps. Technical Report.

1138 Wosten, J., Lilly, A., Nemes, A., Le Bas, C., 1999. Development and use of a database of hydraulic properties
1139 of european soils. Geoderma 90, 169–185.

1140 Zaimes, G.N., Schultz, R.C., Isenhart, T.M., 2008. Total phosphorus concentrations and compaction in
1141 riparian areas under different riparian land-uses of Iowa. Agriculture, Ecosystems and Environment 127,
1142 22–30.

1143 Zellner, M., Garcia, G.A, Bert, F., Massey, D., Nosetto, M. 2020. Exploring reciprocal interactions between
1144 groundwater and land cover decisions in flat agricultural areas and variable climate. Environmental
1145 Modelling & Software, 126, 104641.

1146

Transpiration draws water out of the ground.

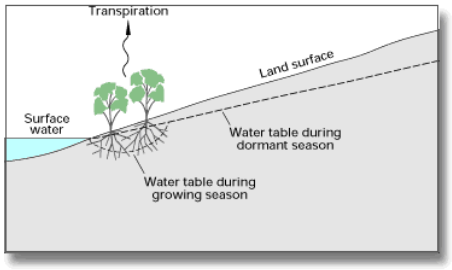

(Public domain.)

Thumbnail Medium Original

Detailed Description

Transpiration and groundwater

In many places, the top layer of the soil where plant roots are located is above the water table and thus is often wet to some extent, but is not totally saturated, as is soil below the water table. The soil above the water table gets wet when it rains as water infiltrates into it from the surface, But, it will dry out without additional precipitation. Since the water table is usually below the depth of the plant roots, the plants are dependent on water supplied by precipitation. As this diagram shows, in places where the water table is near the land surface, such as next to lakes and oceans, plant roots can penetrate into the saturated zone below the water table, allowing the plants to transpire water directly from the groundwater system. Here, transpiration of groundwater commonly results in a drawdown of the water table much like the effect of a pumped well (cone of depression—the dotted line surrounding the plant roots in the diagram).

Details

Image Dimensions: 385 x 233

Location Taken: US

1147

1148

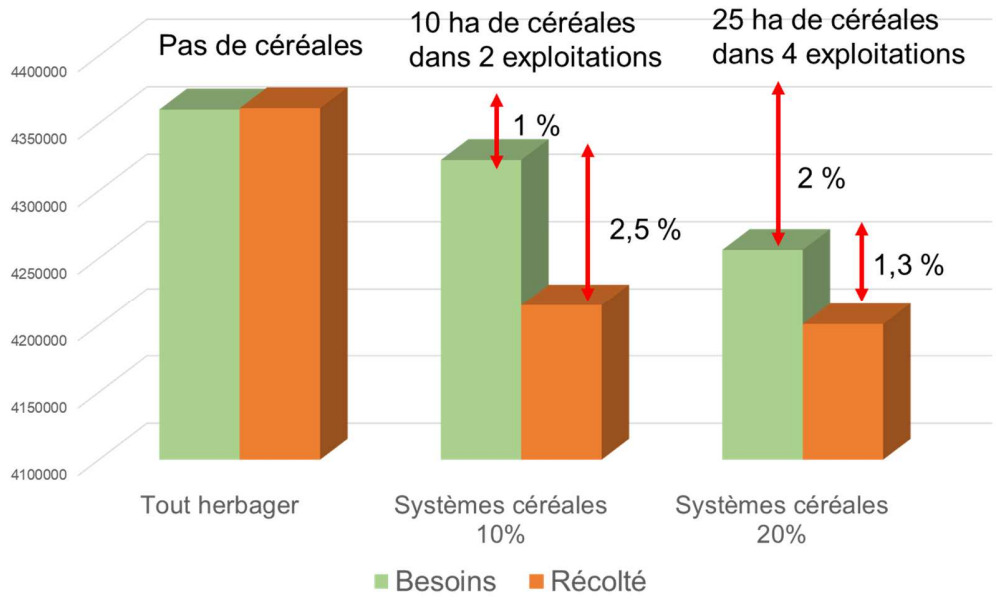

1149

1150 in"C:\Users\admin\Documents\ATemp\Trevisan-Vercors.pptx"

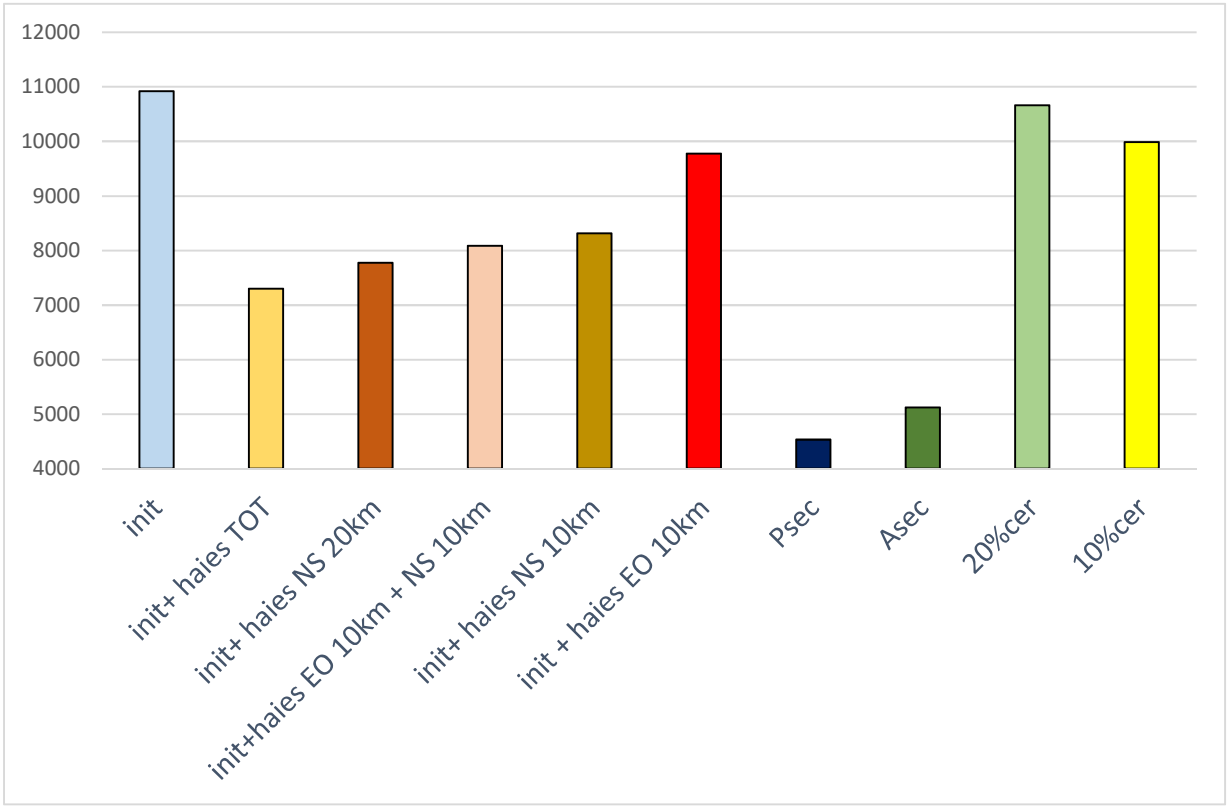

1151

1152 "C:\Users\admin\Documents\Donnees_TIPTOP\ft_autrans_article5.xlsx"